Interleaving of oxygenized intrusions into the Baltic Sea redoxcline

Peter Holtermann [ORCID],* Ralf Prien, Michael Naumann, Lars Umlauf
Leibniz Institute for Baltic Sea Research, Warnemünde, Germany

Abstract

   Semi-enclosed marginal seas like the Baltic Sea are often characterized by permanently anoxic deep layers, and may therefore serve as important model systems to study the causes and consequences of the predicted global expansion of oxygen minimum zones. Here, we focus on the role of lateral intrusions in maintaining the "hypoxic transition zone" (HTZ) of the Baltic Sea, which characterizes the quasi-permanent hypoxic region located between the oxygenized surface layer and the sulfidic deep-water region. Based on long-term deployments of an autonomous profiling system in the central Baltic Sea, we show that oxic mid-water intrusions are ubiquitous features, providing the most important oxygen source for the HTZ, and largely control the vertical and lateral extent of the hypoxic areas. An oxygen budget for the HTZ suggests that oxygen turnover in the HTZ is, to first order, determined by a long-term balance between sedimentary oxygen demand and oxygen import by intrusions. The downward mixing of oxygen into the HTZ is generally non-negligible but unlikely to provide a first-order contribution to the HTZ oxygen budget. On the long-term average, mid-water intrusions were shown to inject 30–60 Gmol of oxygen per year into the deep-water region below the permanent halocline. This is approximately one order of magnitude larger than the average amount of oxygen imported during the massive deep-water inflow events (Major Baltic Inflows) that occur on an approximately decadal time scale, highlighting the HTZ as a hotspot for biogeochemical turnover.

A number of recent studies have drawn attention to a global decrease in the dissolved oxygen content and a rapid spreading of oxygen minimum zones in the ocean with predicted wide-ranging consequences for biogeochemical cycling and aerobic organisms (Stramma et al. 2008; Keeling et al. 2010). While increasing ocean temperatures and other physical factors related to global warming have been identified as the primary reasons for deoxygenation in the open ocean, eutrophication and nutrient recycling were shown to increase the susceptibility of coastal marine systems to hypoxia (Diaz and Rosenberg 2008; Conley et al. 2009b; Breitburg et al. 2018). Semi-enclosed marginal seas like the Baltic Sea, the Black Sea, and the Cariaco Basin, already now characterized by permanently anoxic deep layers, serve as important model systems for understanding the causes and consequences of hypoxia under the extreme conditions predicted for an increasing fraction of the world's marine systems (Astor et al. 2003; Konovalov et al. 2005; Carstensen et al. 2014).

*Correspondence: peter.holtermann@io-warnemuende.de

   For the Baltic Sea, which will be the focus of this study, it has been estimated that the combined effects of eutrophication, nutrient recycling, and climate warming have resulted in a factor-10 expansion of the hypoxic areas over the last century (Conley et al. 2009a; Gustafsson et al. 2012). Massive deep intrusions of oxic waters from the North Sea during the so-called Major Baltic Inflows (MBIs), sporadically occurring on a decadal time scale, are currently believed to be the most important physical factor regulating the temporal and spatial distribution of the anoxic regions. During such MBIs, oxygenated salty (hence dense) waters enter the Western Baltic Sea through the Danish Straits (Fig. 1), and propagate as dense bottom gravity currents through a series of basins and channels until reaching the central Baltic Sea (Stigebrandt 1987; Feistel et al. 2008). Due to their high oxygen content, large volume, and high density, only MBIs have the potential to completely ventilate the anoxic (and often sulfidic) deep layers of the southern and central Baltic Sea (Meier et al. 2006; Gustafsson and Stigebrandt 2007; Holtermann et al. 2017).

   Several experimental investigations carried out in the central Baltic Sea found that such MBIs are generally accompanied by lateral intrusions at intermediate depths, strongly impacting on the local water mass properties inside and below the halocline (Zhurbas and Paka 1997, 1999; Wieczorek et al. 2008; Holtermann et al. 2017). Numerical simulations with models of different complexity (Stigebrandt 1987; Meier and Kauker
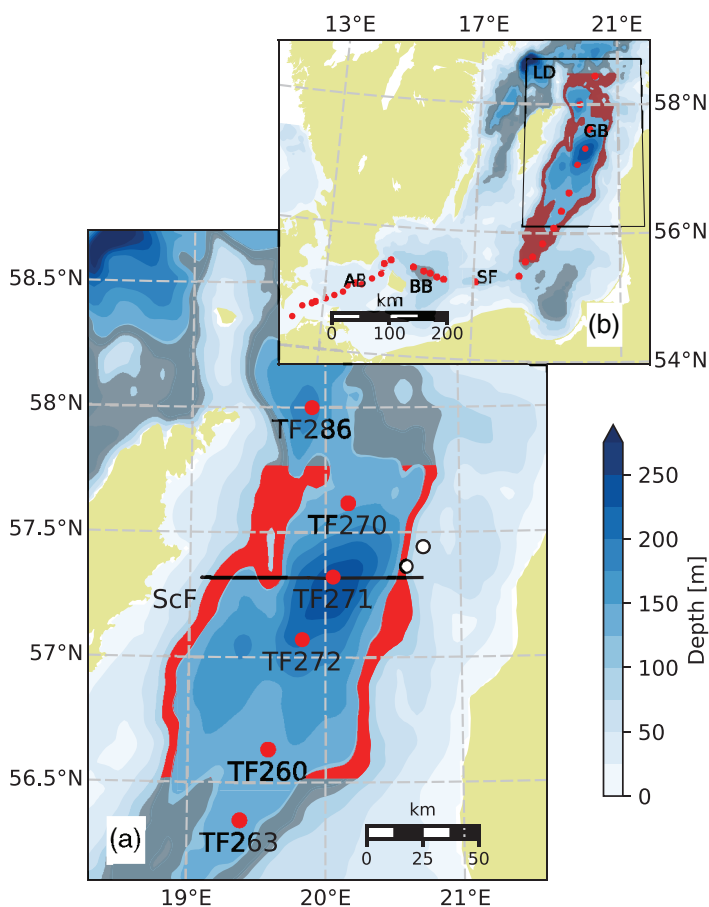
Fig. 1. Maps of (**a**) study area in the Gotland Basin with topography at 25-m intervals, and (**b**) Baltic Sea region overview. The GODESS profiling platform is located in the vicinity of Sta. TF271, close to the deepest point of the basin. Gray-shaded areas indicate the depth range of the HTZ between 90 and 120 m depth. The "central" and "extended" HTZ areas in this depth range (definitions in Table 3) are shaded in red and brown colors, respectively, in panels (**a**) and (**b**). The cross-basin Scanfish transect ("ScF") is depicted as a black line. Red points indicate selected stations of the standard monitoring program, while white points mark the locations of the sedimentary oxygen flux measurements by Noffke et al. (2016). AB, Arkona Basin; BB, Bornholm Basin; SF, Słupsk Furrow; GB, Gotland Basin; LD, Landsort deep.

2003) consistently find that such mid-depth intrusions, rather than being exclusively confined to periods with MBIs, play an essential role also during the long-lasting and much more typical "stagnation periods," when no MBIs are observed. Despite their obvious importance for the overturning circulation and ecosystem functioning, however, mid-depth intrusions have received surprisingly little attention. This may be partly explained by the virtual lack of corresponding observations due to the elusive and strongly intermittent nature of these small-scale features that are hardly resolved with standard CTD monitoring strategies.

Examples from other anoxic systems like the Black Sea and the Cariaco Basin suggest that oxic mid-water intrusions may have a crucial impact on biogeochemical turnover, vertical zonation of redox processes, and the evolution of hypoxic regions. For the Black Sea, it has been shown that lateral injections of oxic Bosporus waters stimulate autotrophic denitrification and induce a chain of oxidation processes that ultimately results in a reduction of the sulfidic areas (Konovalov et al. 2003; Fuchsman et al. 2012). Also for the anoxic Cariaco Basin, it was shown that mid-water intrusions supply additional electron acceptors for organic carbon oxidation near the redox transition zone (Astor et al. 2003; Ho et al. 2004). These findings are in line with a recent Baltic Sea study by Schmale et al. (2016), who showed that turbulent mixing between an oxic near-bottom intrusion and sulfidic ambient waters increased the activity and abundance of methane oxidizing bacteria at the interface between these two water masses.

Here, we show from a new type of high-resolution data, obtained from long-term deployments of an autonomous profiling platform, that small-scale mid-water intrusions are the rule rather than the exception, not only during MBIs but also throughout the usually long-lasting stagnation periods. We argue that the permanent activity of mid-water intrusions is crucial for the maintenance of the hypoxic transition zone (HTZ), typically located just below the halocline. As the HTZ has recently been shown to play a key role for basin-scale nutrient recycling (Noffke et al. 2016; Sommer et al. 2017), the physical mechanisms controlling its variability are of central importance for understanding the long-term ecosystem response to changing nutrient loads.

The article is structured as follows. In Section 1, we give a short introduction to the central Baltic Sea, followed by a description of our oceanographic equipment and methods (Section 2). Within the Results section, an overview about the background and the variability caused by intrusions is given in Section 3.1. The vertical structure of intrusions is discussed in Section 3.2. Section 3.3 presents an algorithm for the identification of intrusions. The vanishing HTZ in 2011 and the absence in 2012 are analyzed in Section 3.4. Section 3.5 gives a multi-basin wide view of the origin of intrusions. The small-scale turbulence and mixing processes in the vicinity of intrusions are discussed in Section 3.6. The results are discussed in Section 4 including a budget (Section 4.1) and an assessment of the long-term role of intrusions (Section 4.2) for the HTZ. Conclusions are found in Section 5.

Study area and hydrography

Figure 1 shows the topography of the Gotland Basin (maximum depth: 248 m), which forms the largest basin of the central Baltic Sea, connected to the more westerly basins via the Słupsk Furrow. For the following discussion, it is important to note that above approximately 130 m depth, the basin is topographically unconstrained. The autonomous profiling station described in more detail below is located near Sta. TF271 in the center of the basin.
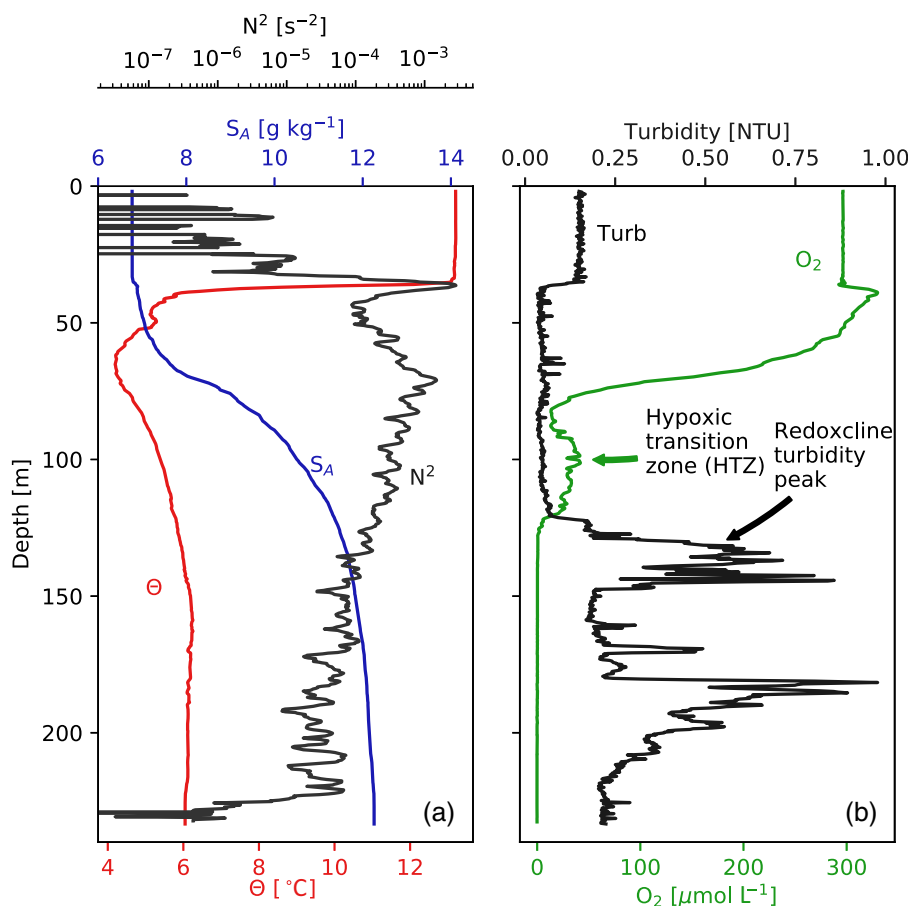
Fig. 2. Profiles of (**a**) conservative temperature, absolute salinity, and squared buoyancy frequency, and (**b**) oxygen and turbidity for a typical stagnation conditions (18 Oct 2014) at Sta. TF271 (Fig. 1). The HTZ and the redoxcline turbidity peak are marked by arrows, respectively.

Typical vertical profiles of the most relevant hydrographic parameters during stagnation conditions are shown in Fig. 2. Immediately evident is the dominant role of the halocline, located between approximately 70 and 90 m depth, in shaping the profile of vertical stratification below the surface layer. During summer and fall conditions (here, a profile from October is shown), a second density interface is generated by the presence of a seasonal thermocline, which separates the warm surface waters from a layer of cold "winter water," extending down to the upper edge of the halocline. As shown by Stigebrandt (1987), deep-water stratification is shaped by the combined effects of dense inflows and vertical turbulent mixing. Because the understanding of mixing in the Baltic Sea was still rudimentary at the time of his study, Stigebrandt (1987) assumed, based on some theoretical arguments for internal-wave dissipation in the ocean (Gargett 1984), that the vertical diffusivity is inversely proportional to the local buoyancy frequency $N = (\partial b/\partial z)^{\frac{1}{2}}$, where b is buoyancy and z the vertical coordinate (positive upward). More recent experimental and numerical investigations of mixing in the Gotland Basin (Holtermann et al. 2012, 2014; Holtermann and Umlauf 2012) showed,

however, that for the deep-water region below the halocline, this model is unlikely to hold, because vertical mixing occurs at the boundaries rather than in the stratified interior of the basin. Boundary mixing is closely coupled to wind-forced topographic and near-inertial internal waves in ways that are incompatible with the model of Stigebrandt (1987).

The profiles in Fig. 2 also show that, as a result of suppressed vertical mixing in the halocline region, oxygen concentrations rapidly decrease from near-saturation values of slightly less than 300 μmol L^{-1} down to approximately 10 μmol L^{-1} in the lower part of the halocline, around 80 m depth. Striking is a slightly deeper local oxygen maximum, centered about 100 m depth, with concentrations peaking around 30 μmol L^{-1}. As shown in the following, the existence of this prominent oxygen peak, evident in most oxygen profiles obtained during stagnation conditions, is closely related to the activity of lateral intrusions. Following previous studies (e.g., Sommer et al. 2017), we will refer to this region as the HTZ. Anoxia in the deepest layers below this HTZ (i.e., below approximately 130 m, *see* Fig. 2b) is typical for the central Baltic Sea, except during the short periods following MBIs. This deepest region is usually characterized by high concentrations of H$_2$S.

Figure 2b also shows that the anoxic side of the transition region (redoxcline) between the oxic and sulfidic waters is characterized by particularly high turbidities. The reasons for this "redoxcline turbidity peak," also reported in earlier Baltic Sea studies (Jakobs et al. 2014) and other anoxic systems like the Black Sea and the Cariaco Basin (Blumenberg et al. 2007; Wakeham et al. 2012), are not entirely understood at the moment. It is clear, however, that this increase in turbidity is not a signal caused by suspended sediment. Based on data from the Baltic Sea and other redoxcline systems, this turbidity anomaly is believed to be the optical signature of colloidal sulfur particles and precipitating metal oxides (Dellwig et al. 2010; Kamyshny et al. 2011). Similar turbidity peaks have also been reported on a smaller scale at the interface between oxic intrusions into sulfidic ambient waters, suggesting that they are generated on relatively short time scales (Schmale et al. 2016; Holtermann et al. 2017). We will come back to this point below.

Numerous studies investigated the evolution of deep-water solute concentrations during MBIs and the following stagnation periods. Typically, these studies are based on solute budgets for the deeper part of the basin below approximately 130 m depth, which is topographically constrained (*see* Fig. 1). It can therefore be argued that, during stagnation periods, vertical mixing is the only physical process affecting the vertical distribution of solutes, which greatly simplifies the construction of closed budgets. The budget method has been used to infer vertical mixing coefficients from the temporal evolution of observed temperature and salinity profiles (e.g., Axell 1998; Holtermann and Umlauf 2012), and, similarly, to quantify the sources and sinks for total carbon (Schneider et al. 2010), and for oxygen, hydrogen sulfide, and some relevant nutrients (Gustafsson and Stigebrandt 2007; Holtermann et al. 2017). In contrast to the deep enclosed part of the basin, the region above approximately 130 m depth (including the HTZ) is virtually always affected by lateral exchange processes, which complicates the application of the budget approach.

Methods

The main instrument used in this study is the Gotland Deep Environmental Sampling Station (GODESS, Prien and Schulz-Bull

2016). GODESS consists of a programmable underwater winch and a buoyant sensor platform attached to the winch via a Kevlar line. At programmed time intervals, the instrument platform ascends with a speed of approximately 0.3 m s^{-1}, and is pulled back after a predefined cable length. As the sensors are mounted on the top of the instrument platform, only measurements obtained during the rising phase will be used in the following. The suite of sensors on the platform differed somewhat over the various deployments: during all deployments, a CTD system (CTD90 from Sea & Sun Technologies, Germany), an optode from JFE Advantech (Japan) for oxygen measurements, and a Seapoint Sensors (U.S.A.) turbidity sensor were installed on the platform. During deployments 11–14, two additional fast FP07 thermistors (Microsquid-T, Rockland Scientific, Canada) for turbulence microstructure observations were added.

Experience has shown that the total number of profiles is usually limited by the battery capacity of the underwater winch, which allows for approximately 200 profiles per deployment. The GODESS system was deployed at 248 m water depth at Sta. P (57°19.20N, 20°08.00E), located at a distance of approximately 5 km from the standard monitoring Sta. TF271 (*see* Fig. 1). The parking depth of the sensor platform was approximately 190–200 m, slightly varying among deployments. To avoid interference with ship traffic, the vertical profiling stopped at 20–30 m below the water surface. Table 1 summarizes the GODESS deployments analyzed in the following (times are reported in UTC throughout this document).

In addition to the GODESS measurements, full-depth vertical profiles of hydrographic variables were obtained with a SBE 911plus CTD package (Sea Bird Scientific, U.S.A.) during research and regular monitoring cruises, which are conducted on a bimonthly basis by our institute. This package also included SBE-43 oxygen sensors from Seabird. From 2008 onward, the CTD system was equipped with double-sensor packages for temperature, conductivity, and oxygen, which greatly increased our ability to estimate measurement uncertainties, in particular with regard to oxygen concentrations. For this reason, the analysis of oxygen variability in the HTZ will exclusively be based on quality-controlled data (see below) from periods with double-sensor

Table 1. Summary of GODESS deployments in the Gotland Basin at Sta. P in 248 m water depth.

Deployment	First profile	Last profile	Profiles	Interval
2	03 Jul 2010 18:00	05 Aug 2010 10:00	198	4 h
3	16 Nov 2010 22:00	11 Jan 2011 14:00	170	8 h
5	30 Jun 2012 18:00	18 Jul 2012 23:00	184	2.4 h
8	09 Nov 2013 05:00	30 Nov 2013 00:00	61	8 h
10	15 Aug 2014 10:00	11 Sep 2014 18:00	77	8 h
11	07 Dec 2014 10:00	08 Jan 2015 18:00	92	8 h
12	28 Feb 2015 11:00	05 Mar 2015 05:00	39	3 h
13	05 Mar 2015 18:00	19 Apr 2015 06:00	90	12 h
14	21 Apr 2015 20:00	18 Jul 2015 18:00	89	24 h
15	26 Jul 2015 18:00	24 Sep 2015 09:00	159	9 h
17	29 Oct 2015 04:00	31 Jan 2016 20:00	143	16 h

packages. Beyond vertical CTD profiling at fixed stations, we also performed measurements along transects through the Gotland Basin down to a depth of approximately 140 m, using a towed and undulating "Scanfish" CTD system (EIVA, Denmark), equipped with an SBE 911plus CTD in a single-sensor configuration, including an SBE-43. Throughout this document, temperatures and salinities are reported as conservative temperature Θ and absolute salinity S_A, including a correction for the Baltic Sea salinity anomaly according to the international TEOS-10 standard (Millero et al. 2008; Feistel et al. 2010). Please note that in the Baltic Sea, differences between Θ and the in situ temperature may be of order of 0.1 K, depending on depth.

Sensors from all systems were regularly calibrated at the institute's certified calibration lab. From the sensor drift between calibrations, effective measurement uncertainties of 0.003 K for temperature and 0.01 mS cm^{-1} for conductivity were determined. The measurement uncertainty for oxygen (both SBE-43 and JFE Advantech optode), as given by the manufacturer of the sensors, is 2% of the saturation concentration (i.e., 7 μmol L^{-1} for oxygen saturated water with a salinity of 6 g kg^{-1} and a temperature of 10°C). Due to the anoxic deep water, it was possible to remove the zero-point offset for every cast. Between deployments 10 and 12, during which the same JFE Advantech optode was used with the same calibration coefficients, the offset showed a slight increase from −4.1 to −1.8 μmol L^{-1}. The offsets between individual casts within a deployment varied with a standard deviation of not more than 0.15 μmol L^{-1}. A careful comparison of the two oxygen sensors from the SBE-43 double-sensor package for the years 2011/2012 (the key period for our analysis) revealed a maximum difference of only ± 1 μmol L^{-1} within the hypoxic zone, the measurement uncertainty is therefore unlikely larger than 1 μmol L^{-1} for the double-sensor CTD system. As shown below, this is sufficient to reliably estimate oxygen decay rates in the HTZ, where oxygen concentrations are typically one order of magnitude larger than the measurement uncertainty. Monitoring data before 2008 were not used for our analysis of the HTZ as measurement uncertainties were possibly too large. This was partly due to the lack of double-sensor packages, and partly because earlier generations of oxygen sensors (SBE13/23, Sea Bird Scientific) turned "blind" after first contact with hydrogen sulfide. This made it virtually impossible to detect oxic intrusions within sulfidic water.

Turbidity sensors were not calibrated, and could therefore only used qualitatively in our study. During GODESS deployment 10, the turbidity sensor was misaligned and the reflections from the instrument frame affected the readings. This resulted in a slight turbidity offset that did, however, not influence the detection of turbidity fluctuations due to intrusions.

Results
Background conditions and variability due to intrusions

Temperature, salinity, oxygen, and turbidity of all GODESS deployments between 2010 and 2016 are shown in Fig. 3 for the first four nonconsecutive deployments, and in Fig. 4 for the almost contiguous deployments between 2014 and 2016. Salinity profiles (Figs. 3a and 4a) show the typical large-scale stratification pattern for the central Baltic Sea with a dominant halocline in approximately 80 m depth. Density contours closely trace the haline stratification as the effect of temperature on density is generally small (*see* also Section 3.2).

In contrast to the pronounced seasonality of the temperature above the halocline (Figs. 3b and 4b), the deeper layers show no obvious seasonal pattern. Virtually all deployments, however, exhibit irregular temperature fluctuations due to intrusions at depths between the halocline and the bottom. These anomalies, most pronounced in deployment 3, are generally colder than the average, and accompanied by either oxygen or turbidity anomalies. Distinct examples for correlated fluctuations in temperature and turbidity can be identified below approximately 130 m in July/August 2010 (deployment 2). Similarly, correlated temperature and oxygen fluctuations are observed in the HTZ below the halocline throughout deployment 3 (Fig. 3). Oxygen concentrations in the deeper layers below approximately 150 m depth are zero for deployments 2–8 (Figs. 3c and 4c), indicating a classical "stagnation period" during this time. Between deployments 8 and 10 (March 2014 to August 2014), a weak MBI entered the basin, transporting water masses with oxygen concentrations of up to 24 μmol L^{-1}, which caused a subsequent decrease of hydrogen sulfide from 138.4 μmol L^{-1} to zero. This MBI interrupted a stagnation period that started more than a decade ago in 2003 (Naumann et al. 2017). The very strong MBI of December 2014, which reached the Gotland Basin in March 2015 and ventilated the deepest layers of the Gotland Basin, provided oxygen for a period of approximately one year (deployments 12–17). The evolution of this MBI and its consequences for the oxygen budget and deep-water mixing processes are discussed in detail in Holtermann et al. (2017).

Here, we focus on the effect of intrusions at the intermediate depth levels of the HTZ and the layers below. For the following analysis, it is helpful to note that the 130 m isobath approximately delineates the deeper, enclosed part of the Gotland Basin (Fig. 1). This depth level typically also marks the lower edge of the HTZ, with the exception of deployment 5, during which the HTZ vanished completely. The special conditions leading to this exceptional situation will be exploited below to compute oxygen decay rates for the HTZ.

Characterization of intrusions

The observations shown in Figs. 3 and 4 suggest that intrusions in the central Baltic Sea can be differentiated from the surrounding waters by several distinct features. They usually exhibit pronounced temperature anomalies, and are characterized by either higher oxygen concentrations or, in anoxic conditions, higher turbidities. As discussed above, the latter are likely representing the optical signature of colloidal particles formed in the vicinity of strong redox gradients. These anomalies may therefore indicate the final stage of formerly oxic
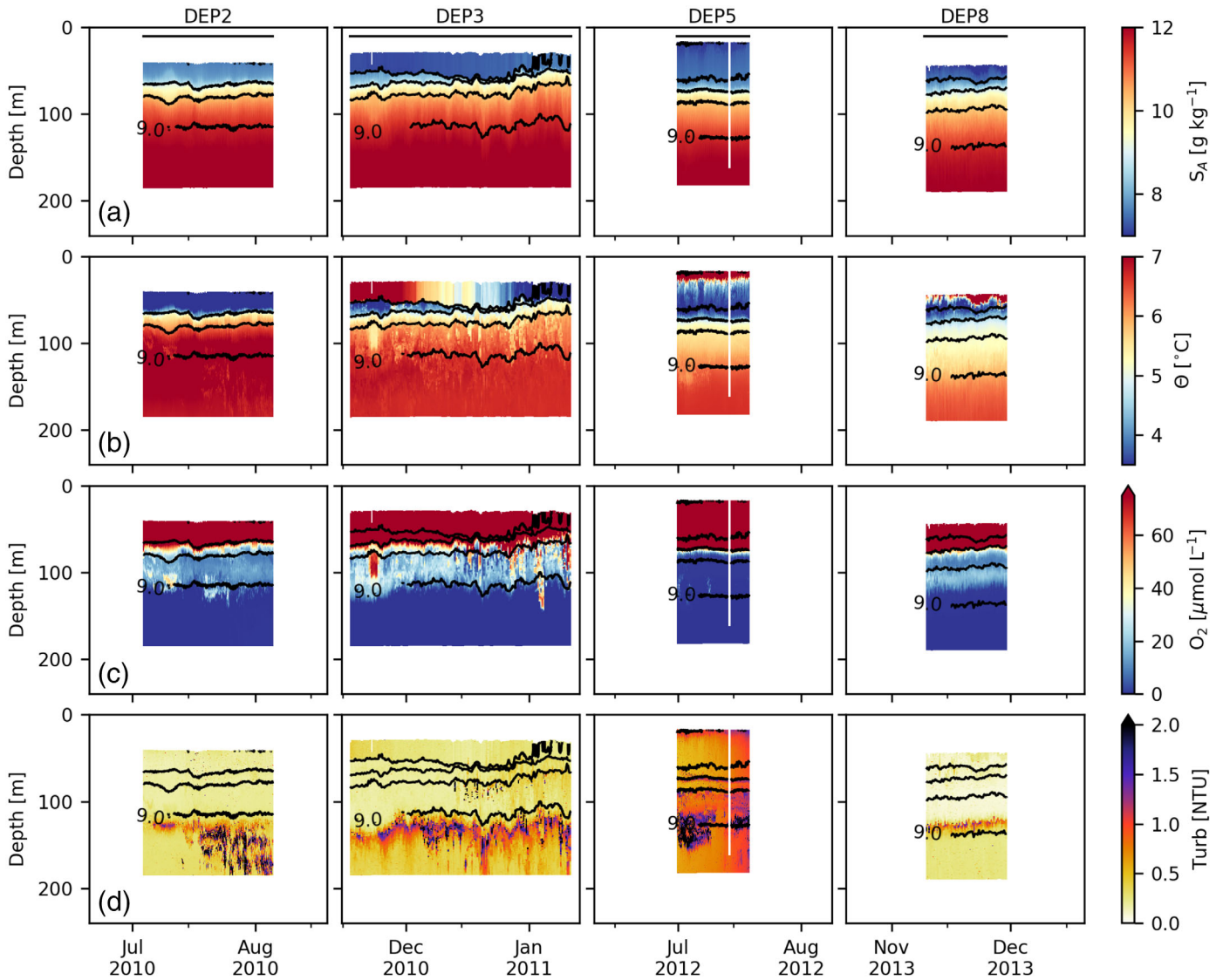
Fig. 3. GODESS profiles of (**a**) salinity, (**b**) temperature, (**c**) oxygen, and (**d**) turbidity for deployments 2–8. Black contour lines indicate potential density at 1.0 kg m^{-3} intervals. Note the large gaps in the time axis.

intrusions that have lost their oxygen on their pathway through anoxic ambient waters (e.g., Schmale et al. 2016). Irrespective of the exact mechanisms involved in this process, it should be clear that the enhanced turbidities in this type of intrusions provide a robust indicator for their identification.

Deployment 3 overlapped with a period of particularly clear examples for the first type of intrusions, in this case associated with negative temperature anomalies and high oxygen concentrations in the depth range between the halocline and 135 m depth (Fig. 3). Numerous examples for the second type of intrusions (zero oxygen, enhanced turbidity) can be identified in the deeper anoxic regions in deployments 2 and 3. Both types of intrusions are typically vertically coherent over distances of order 1–10 m, and periods ranging from days to approximately 1 week maximum. Sporadic ship surveys (including those from the institutes standard monitoring

program for the Baltic Sea) are therefore unlikely to resolve the spatial and temporal coherency of these features (Meyer et al. 2018), which may explain why they have remained largely unnoticed so far.

Figure 5, based on a single GODESS profile taken during deployment 2, provides a more detailed view of the vertical variability induced by these different types of intrusions. As an indicator for the undisturbed background conditions, this figure also includes isopycnal averages of all quantities, taken over all profiles of this deployment and plotted against the average depth of the corresponding isopycnal (*see* Section 3.3 for more details about the averaging procedure). Figure 5e–h, focusing on the hypoxic and anoxic zones below the halocline, show clear evidence for both types of intrusions. Intrusions of the first type (correlated temperature and oxygen anomalies) can be identified in the hypoxic depth range between 100 and 135 m, where
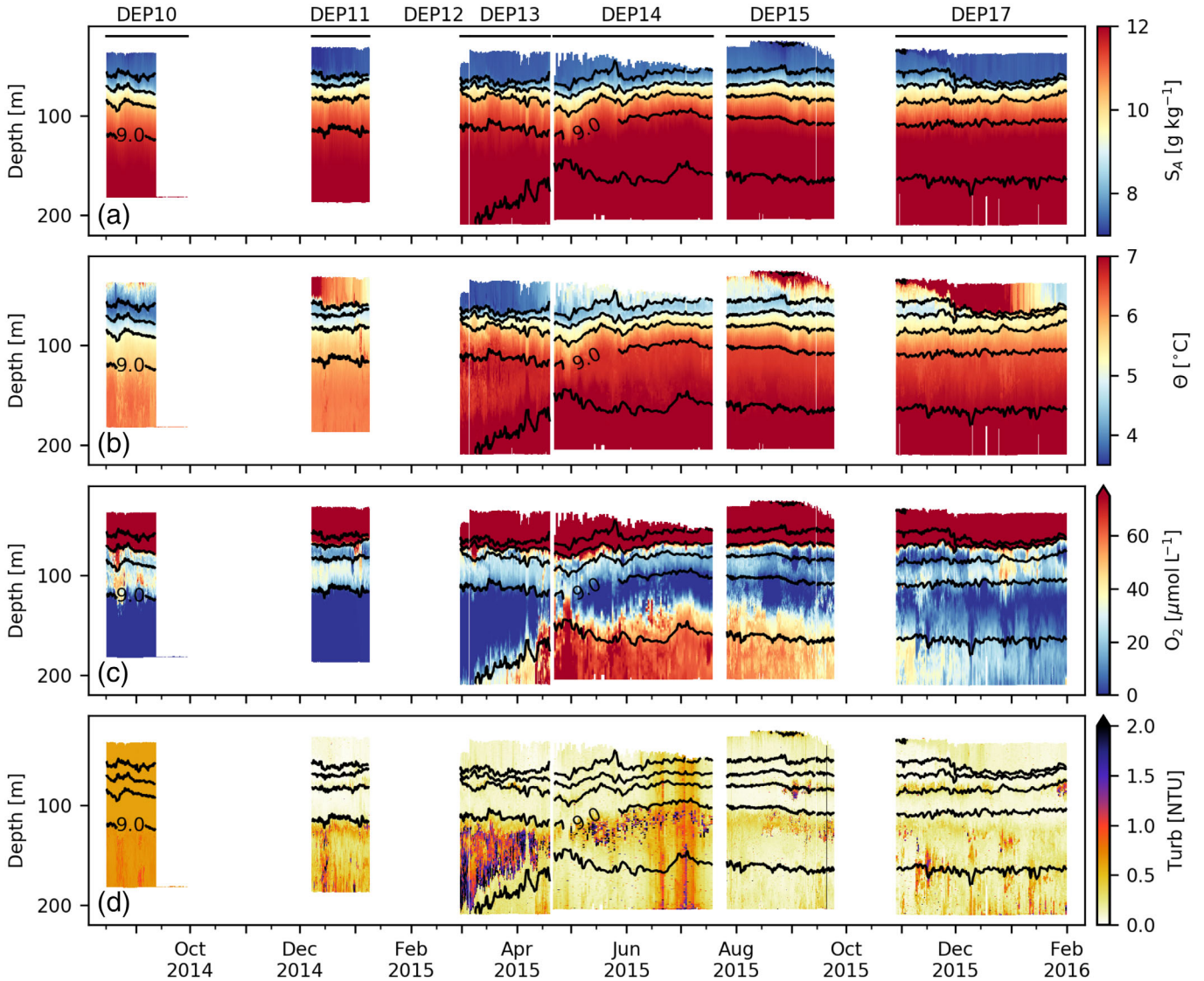
Fig. 4. As in Fig. 3 but now for deployments 10–17.

temperatures are approximately 0.5 K colder than the isopycnal average, and small-scale temperature fluctuations of the same order of magnitude are observed. In this region, the ratio of the thermal expansion coefficient α and the haline contraction coefficient β is only $\alpha/\beta \approx 0.08$ g kg^{-1} K^{-1}, suggesting that salinity variations of only a few times 0.01 g kg^{-1} are required to compensate the effect of the observed temperature fluctuations on density. This is consistent with the magnitude of the negative salinity anomalies associated with the cold intrusions shown in Fig. 5e. The intruding waters thus approximately follow surfaces of constant salinity. Oxygen concentrations inside the cold intruding waters are of the order of 10 μmol L^{-1} elevated above the background level (Fig. 5g), pointing at their potential importance in maintaining the HTZ.

Evidence for the presence of the second type of intrusions (correlated temperature and turbidity anomalies) can be found in the anoxic layers below 135 m depth. There, centered at 158 m depth, a 10–15 m thick intrusion of cold and turbid waters can be identified, clearly decoupled from the "classical" redoxcline turbidity peak in the transition region between the oxic and anoxic waters approximately 20 m higher up in the water column. Temperature anomalies and turbidities in this case are 0.2–0.3 K and 2–3 NTU relative to their isopycnal averages, respectively. Note that the oxic waters above approximately 135 m show no discernible turbidity anomalies.

Identification of intrusions

Based on the typical features of intrusions identified above, an algorithm for their identification can be constructed. To this end, we first define, for each variable, a relevant background state corresponding to the isopycnal average $\langle \cdots \rangle_\sigma$ over all profiles per deployment. For each profile and variable,
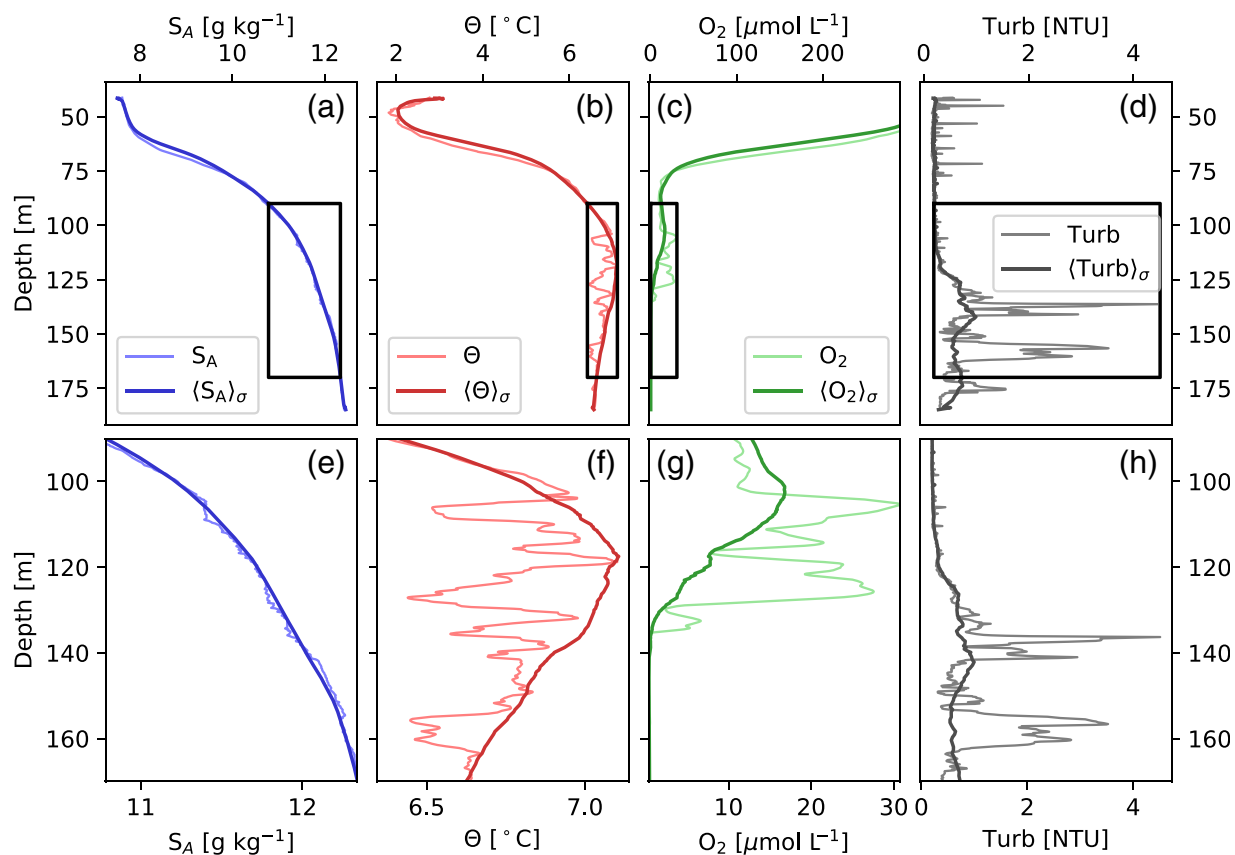
Fig. 5. Profile of GODESS deployment 2, obtained on the 19 Jul 2010 at 21:57 UTC. Panels (**e**)–(**h**) show an enlarged view of the region delineated by the black rectangles in panels (**a**)–(**d**). Light colors correspond to individual profiles while dark colors denote the corresponding isopycnal averages taken over all profiles of this deployment.

we then compute profiles of the anomalies with respect to the background state. These anomaly profiles may contain regions affected by intrusions if the anomalies of both temperature and oxygen (or, in the case of anoxic intrusions, temperature and turbidity) simultaneously exceed predefined thresholds.

The data presented above suggest that the detection threshold for temperature anomalies should be of the order of 0.1 K. Unsurprisingly, it turned out that the algorithm is sensitive with respect to the exact value of the temperature threshold if the detection of intrusions is exclusively based on this parameter. Taking deployment 2 as an example, the number of data points detected as intrusions in the depth range below 80 m increased by a factor of 2.5 if the threshold was halved from 0.1 to 0.05 K. However, combining the temperature criterion with a threshold of 2 μmol L^{-1} for positive oxygen anomalies (or a positive turbidity threshold of 1 NTU for anoxic conditions) mitigates the strong temperature dependence to a factor of 1.4. We therefore assume in the following that a subregion of a vertical profile is affected by intrusions if it shows a temperature anomaly exceeding 0.1 K and, simultaneously, a positive oxygen anomaly of more than 2 μmol L^{-1}, or, in the case of anoxic intrusions, a positive turbidity anomaly of more than 1 NTU. Clearly, these thresholds are to some extent

arbitrary. The following results, however, turned out to be not overly sensitive with respect to the exact values, and the detected intrusions coincide with those identified from visual inspection.

Using deployment 2 as an example, Fig. 6 shows that the intrusive regions detected with this choice of thresholds closely coincide with those found by visual inspection. Temperature anomalies associated with intrusions are generally negative (cold intrusions) for this deployment, and extend over the entire profiling range below the halocline (Fig. 6b). The imprint of the oxic/anoxic interface at approximately 135 m depth is clearly discernible in the vertical zonation of the two types of intrusions defined above: intrusions above the redoxcline generally import oxic waters (Fig. 6d), whereas those in deeper layers are typically anoxic and characterized by increased turbidity (Fig. 6f). Note, however, that occasionally (e.g., in the second and third week of July) oxic intrusions may penetrate into the anoxic layers (Fig. 6c), pointing at their potential importance for the regulation of the redoxcline depth.

The abundance and distribution of the different types of intrusions for all deployments are quantified in Fig. 7, which shows, for every depth level, the fraction of profiles during which intrusions were detected. This figure reveals that

intrusions at intermediate depth levels are ubiquitous features that may be observed up to 20% of the time, with a particularly strong intrusion activity found during deployments 2, 3, and 10. The profile for deployment 10 (August/September 2014) seems to indicate that oxic intrusions are strongly reduced above approximately 110 m, which is obviously inconsistent with Fig. 4c, showing clear indications for oxic intrusions above this level. Comparison with Fig. 4b shows, however, that this period corresponded to a rather special situation, in which intruding and ambient waters had nearly identical temperatures. Such intrusions are not correctly identified by our algorithm, suggesting that the profiles in Fig. 7 provide lower bounds for the occurrence of intrusions.

Figure 7 shows that the character of intrusions generally changes from type 1 (oxic) to type 2 (anoxic/turbid) around the redoxcline level, which varies among different deployments. In many cases, there is an overlap region affected by both types of intrusions, which does, however, not imply that intrusions of different types coexist at the same time. Similar to the example shown in Fig. 6c (see above), the overlap region mirrors the average effect of sporadic intrusion of oxic waters into the sulfidic layers below the oxic/anoxic interface. Note that type 2 intrusions may occasionally extend down to the lower measurement range of the profiling system, suggesting that they have the potential to affect even the deepest anoxic layers.

Figure 7 also shows that deployment 5 (July 2012) exhibits a special situation with exceptionally weak oxic intrusions, and a complete lack of intrusions in the depth range between the halocline and approximately 110 m depth. This unusual period coincides with a vanishing of the HTZ, and a resulting expansion of the deep anoxic region up to the lower edge of the halocline (Fig. 3). This deployment therefore provides some direct evidence for the importance of oxic intrusions in maintaining the suboxic zone, which has far reaching consequences and therefore deserves a closer investigation.

Collapse of the HTZ in 2011 and 2012

As deployment 5 was only of short duration, we combine our sparse GODESS measurements with additional CTD profiles taken at the nearby Sta. TF271 between 2008 and 2014 (i.e., just before the MBI mentioned above) during our institute's regular monitoring cruises. As discussed in Section 2, our analysis will be exclusively based on oxygen data from periods with double oxygen sensor packages, as measurement uncertainties from other oxygen measurements turned out to be too large for the computation of reliable oxygen budgets in the HTZ.

Figures 3c and 4c show that, in all deployments, the HTZ below the halocline is approximately delineated by the isopycnals at 8.0 and 9.0 kg m^{-3}. In the following, we therefore use the location of the intermediate 8.5 kg m^{-3} isopycnal
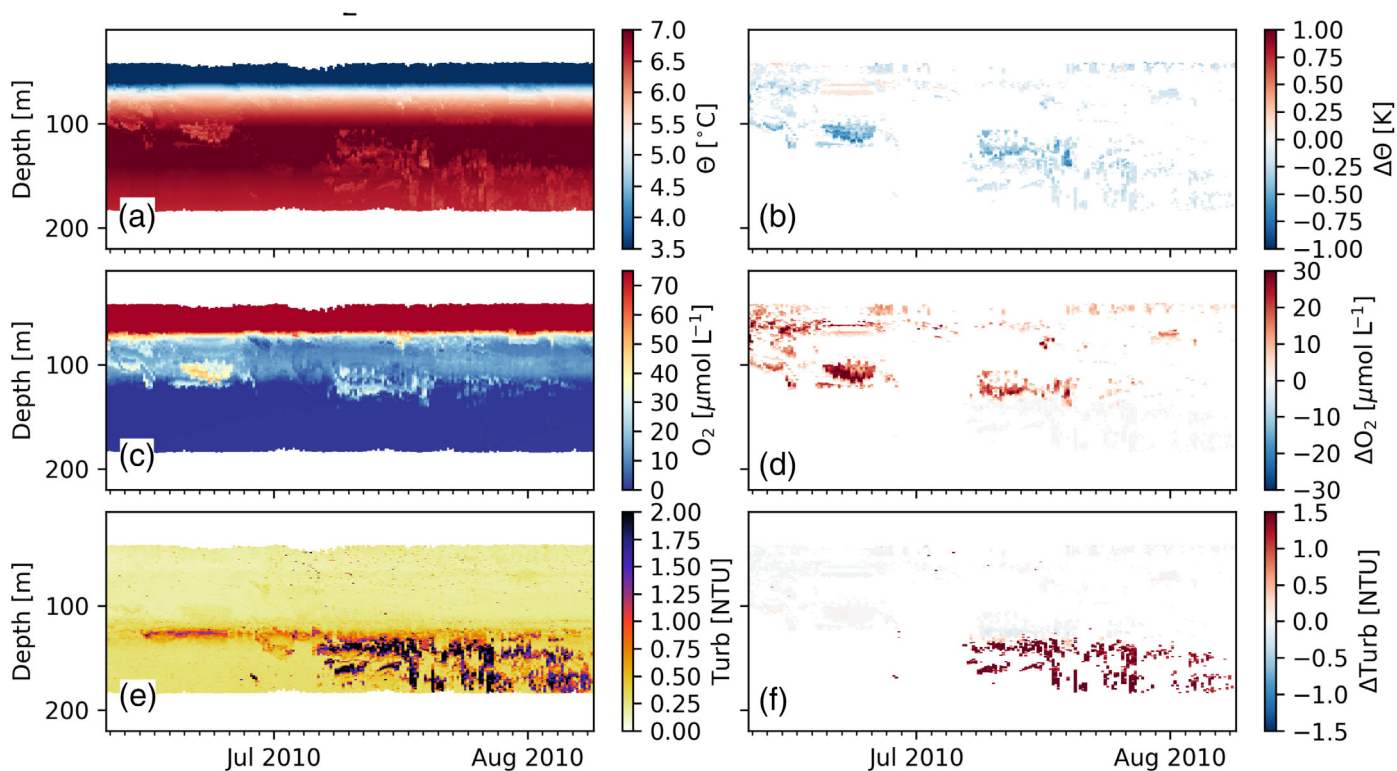

Fig. 6. Variability of (**a**) conservative temperature, (**c**) oxygen, and (**e**) turbidity during deployment 2 (*see* Fig. 3). Panels (**b**), (**d**), and (**f**) show the corresponding anomalies, where regions below the detection thresholds for intrusions (see main text) have been blanked. Light gray-shaded areas in (**d**) indicate intrusions below the threshold for oxygen anomalies but above that for turbidity, and vice-versa for panel (**f**).
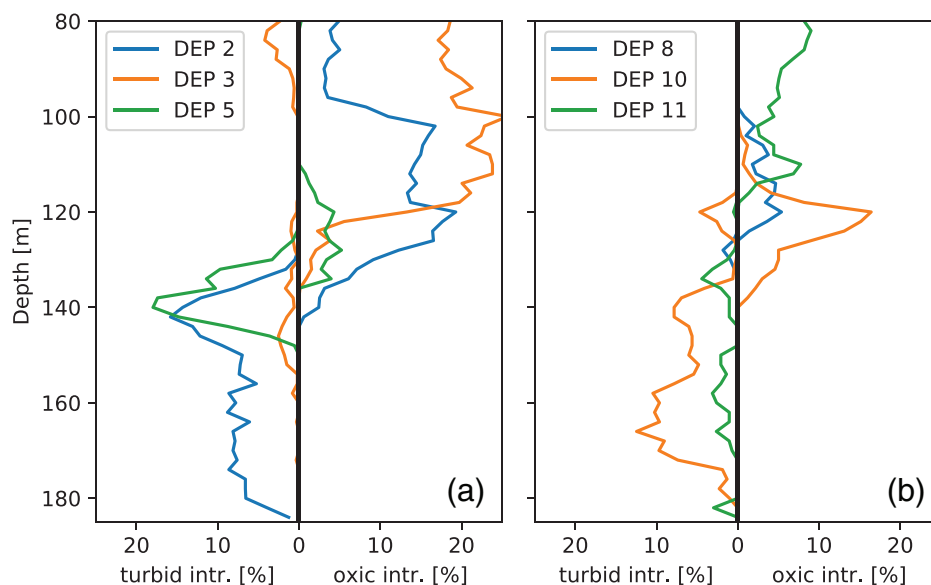
Fig. 7. Fraction of time per deployment intrusions have been detected, differentiating between oxic and anoxic/turbid intrusions. Colors indicate different deployments.

to represent some bulk properties of the HTZ. As vertical isopycnal excursions due to internal waves and other physical processes affect the vertical position of the HTZ, this isopycnal was found to reflect the conditions in the HTZ better than a fixed depth level. Time series of temperature and oxygen concentrations at the depth of the 8.5 kg m^{-3} isopycnal are shown in Fig. 8 for the period 2008–2014. These data show that the unusual disappearance of the HTZ identified in

deployment 5 extended over a 1-year period between fall 2011 and fall of 2012, that is, much beyond the small time window of deployment 5. Inspection of a 37-year time series of H$_2$S data from our and the Swedish monitoring program at Sta. TF271 between 1980 and 2017 (not shown) revealed non-zero H$_2$S concentrations at 100-m depth (used as a proxy for the depth of the HTZ) only during 2012 and a single additional event in 2004. Thus, although the interpretation of the data is
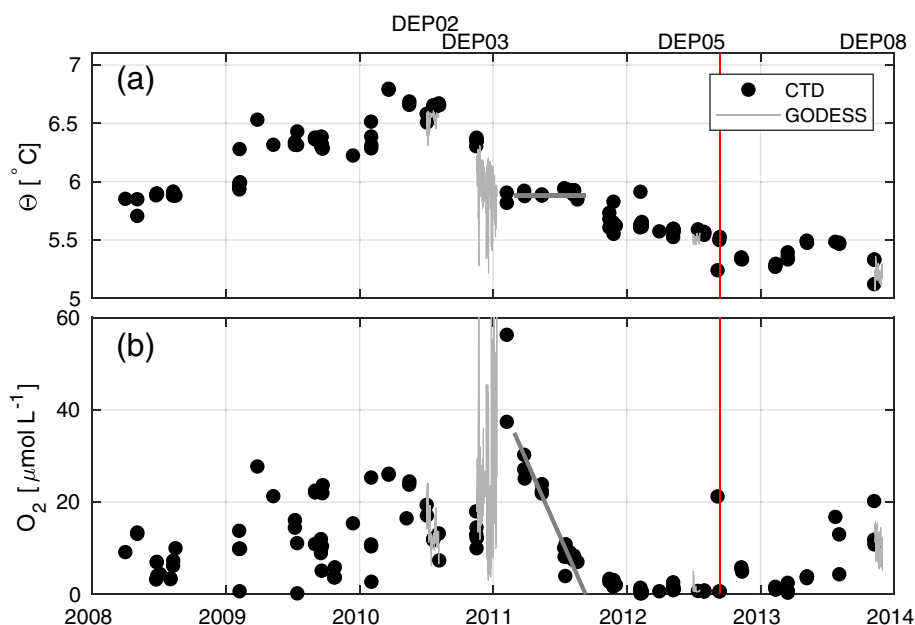

Fig. 8. Time series of (**a**) temperature and (**b**) oxygen at the potential density of 8.5 kg m^{-3} at Sta. TF271. The depth of this isopycnal varies between 90 and 125 m over the period displayed here. Black solid points indicate CTD measurements at position TF271; gray lines correspond to data from GODESS deployments. The red line marks the date of the Scanfish transect shown in Fig. 10. Thick gray lines indicate trends of temperature and oxygen in 2011.
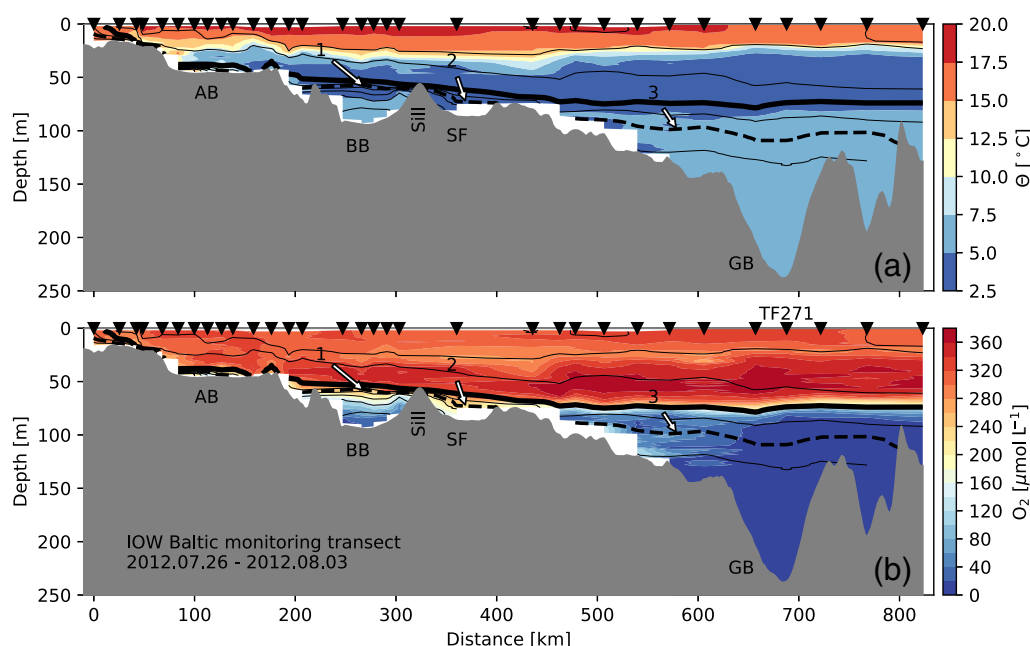
Fig. 9. Temperature (**a**), and oxygen (**b**) along a transect of the western and central Baltic Sea taken during a regular monitoring cruise in Jul/Aug 2012. See Fig. 1a for the location of the stations. The thick black contour line shows a potential density of 7.0 kg m^{-3}. Density difference between contours is 1.0 kg m^{-3}. Thick dashed line shows the density at 8.5 kg m^{-3}.

somewhat limited due to their coarse vertical resolution and sparseness at the beginning of the record, this suggests that the vanishing of the HTZ below the halocline is a rare event.

The collapse of the HTZ was preceded by a period with continuously decreasing oxygen concentrations from almost 40 μmol L^{-1} in January 2011 down to zero in December 2011. This decrease showed a nearly linear trend during the summer periods with a decay rate of 0.18 μmol L^{-1} d^{-1} (Fig. 8b). A detailed analysis of all available CTD profiles for this period (*see* Supplementary Material) showed no indications for a significant lateral import of oxygen by intrusions. Moreover, temperatures on the 8.5 kg m^{-3} isopycnal generally stagnated during the summer months, which is particularly evident for the year 2011 (Fig. 8a). This suggests that significant vertical mixing is confined to the winter months, consistent with earlier studies by Axell (1998) and Holtermann and Umlauf (2012), who showed a similar seasonality of mixing for the deeper layers of the Gotland Basin. From the lack of significant lateral intrusions and mixing, it thus follows that the decreasing oxygen concentrations in the HTZ largely result from biogeochemical oxygen consumption, including the sedimentary oxygen demand. We will use this argument later to construct an oxygen budget for the hypoxic zone, from which the total amount of oxygen imported by intrusions on the long-term average can be estimated. Parallel to the decreasing oxygen concentrations in 2011, the anoxic deep-water volume gradually expanded, and reached a depth of approximately 80 m, just below the halocline, in January 2012.

In September 2012 (red line in Fig. 8), a warm and oxygen-rich intrusion entered the zone below the halocline which was

at this time still anoxic. The lateral structure of this intrusion is discussed in Section 3.5 below. The HTZ was reestablished in February 2013, reaching depths of 120 m in March 2013.

The origin and pathways of intrusions

The origin of the measured intrusions can be traced back to the dense water of the deeper Bornholm Basin, which itself originates from the Arkona Basin (Reissmann et al. 2009). This water, when lifted above the sill between the Bornholm Basin and the Słupsk Furrow, will interleave at its equilibrium depth, or form a dense bottom gravity current. Here, we will discuss two instructive data sets from July/August 2012 and September 2012, which can be considered snapshots of situations directly before the arrival of the intrusions in the Gotland Basin. The absence of the HTZ in 2012 made oxic intrusions entering into purely anoxic water particularly easy to distinguish from the surroundings. The available measurements in 2012 showed only one significant intrusion event, which was not able to reestablish the HTZ, but provides some insights into the pathway and lateral structure of intrusions from the Bornholm Basin toward the Gotland Basin. In July/August 2012, a regular monitoring cruises through the Baltic Sea (*see* Fig. 1 for the location of the stations) showed no oxygen in the depth range of the HTZ at TF271 (Fig. 9b). Nevertheless, if the 8.5 kg m^{-3} isopycnal is followed from the west in the Bornholm Basin (arrow "1" in Fig. 9), to TF271, it can be nicely observed that the water in the Bornholm Basin is colder, oxygen richer, and the vertical distance of the isopycnal to the halocline decreased strongly compared to
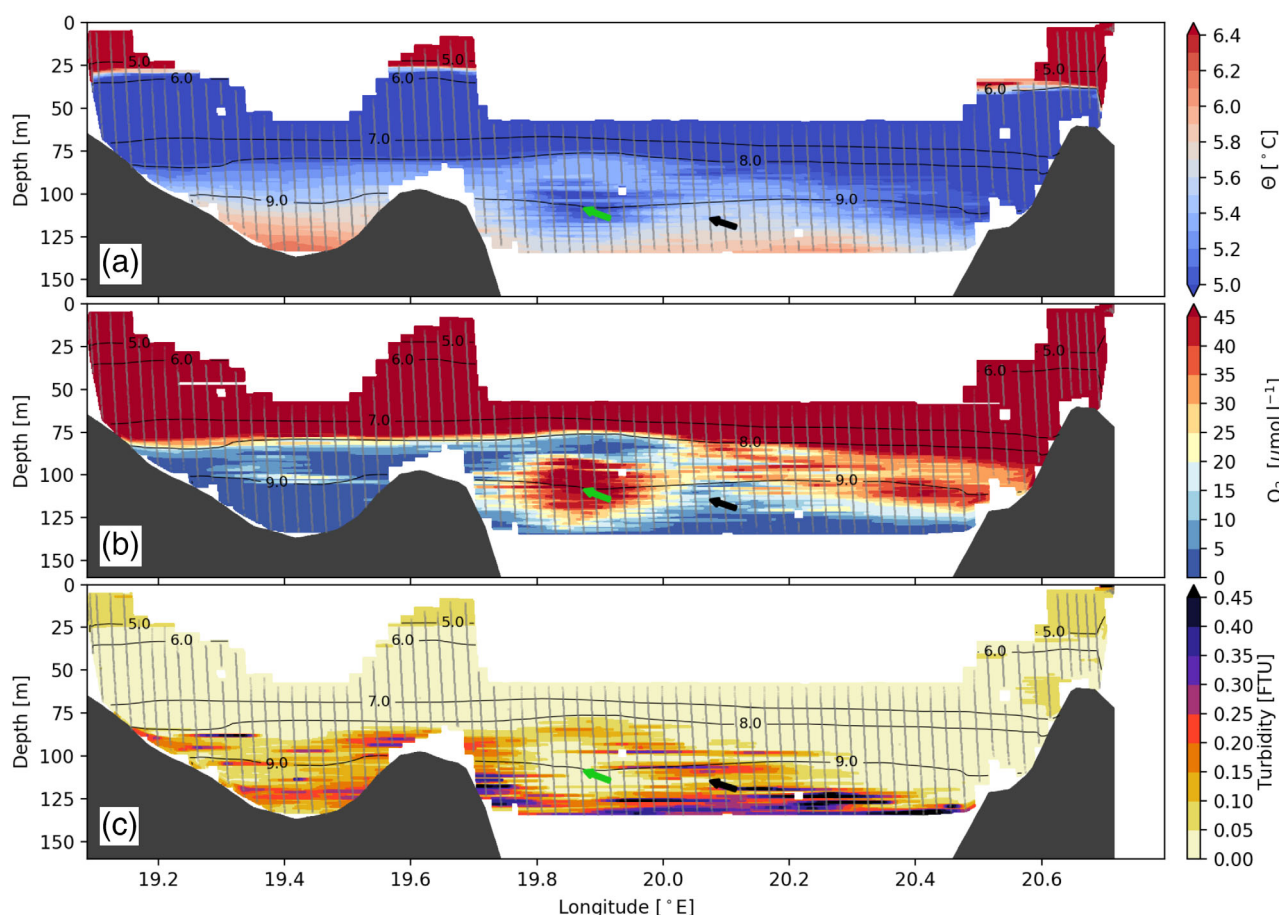
Fig. 10. Temperature (**a**), oxygen (**b**), and turbidity (**c**) of a Scanfish transect through the Gotland Basin during the AL400 cruise. The transect started on the eastern side on the 11 Sep 2012, 17:09 and ended on the western side on 12 Sep 2012. Black dots mark the measurements. Black contours show isopycnals of potential density. Green arrow depicts a pronounced, black arrow a thinner layered, intrusion.

TF271. In the Bornholm Basin, the halocline depth is similar to the sill height between the basin and the Słupsk Furrow. If this dense and oxygen rich water is lifted above the sill, it will enter the Słupsk Furrow (arrow "2"). The water, when it is denser than the surrounding water, will continue downhill toward the Gotland Basin. On the way, it will mix with the surrounding water, resulting in a larger vertical distance between the isopycnal and the halocline. The mixing of the dense water with the less oxygenized surrounding water is at the same time decreasing the oxygen concentration of the intrusion. At arrow "3," the continuation of this process can be observed. The transect shows that the intrusions did almost reach the central station, signs of intrusions into the HTZ can be found in 50 km distance of TF271.

Just a month after the transect of the Baltic Sea monitoring program, a campaign in the Gotland Basin included Scanfish transects through the basin, *see* Fig. 1 for the location and Fig. 10 for the data. The data show that in between the time of the two cruises, the intrusions prominently entered the Gotland Basin. The water below 80 m on the western side of the basin has temperatures above 5.6°C, Fig. 10a. On the

central and eastern part of the basin cold water with 5.0°C is interleaving into the warmer surrounding water, see also green arrows in Fig. 10. The cold water of the intrusion is accompanied by oxygen and is much clearer than the surrounding water, as seen in the turbidity in Fig. 10c. This transect is also a useful example to explain the temporal variability of temperature, oxygen, and turbidity seen in the GODESS data above, as due to the movement of the water, the intrusions with their different properties will be advected past the GODESS mooring. A second example of intruding water is marked with black arrows. Here also, an interleaving of the intrusions with the warmer and anoxic water can be observed, but with a much smaller ratio of intruding water to the surrounding water. That this intrusion was a singular event without a succession of intrusions can be seen in the oxygen concentration after summer 2012 (Fig. 8). The oxygen imported by the intrusion decreased and the water became anoxic again in winter 2013.

Turbulence and mixing in the vicinity of intrusions

During deployment 11 (November 2014–January 2015), the profiling platform was equipped with temperature
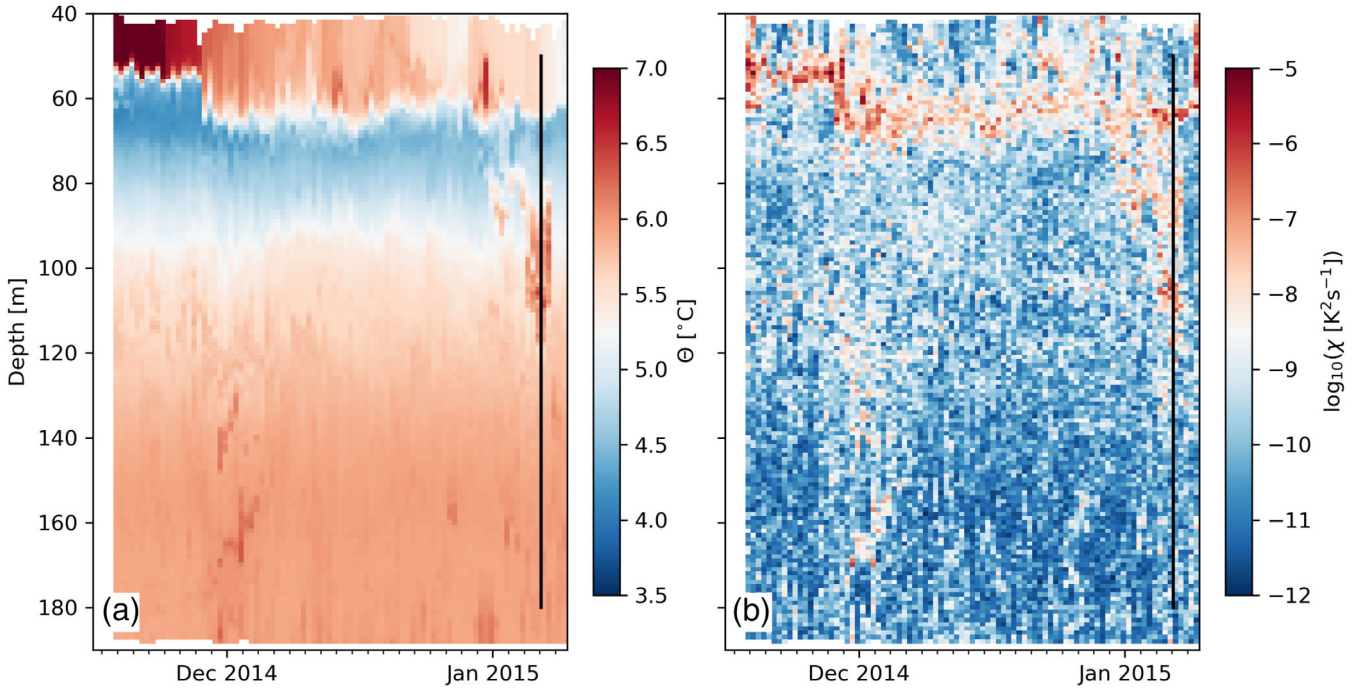
Fig. 11. Variability of (**a**) temperature and (**b**) temperature variance decay rate during deployment 11. Note that only a part of the water column is shown. The black line indicates the profile analyzed in Fig. 12.

microstructure sensors, resolving temperature fluctuations down to vertical scales of order 0.01 m. Useful information about mixing processes, mixing parameters, and energy dissipation in the HTZ and in the vicinity of intrusions can be inferred from these data, as discussed in the following.

The temperature microstructure data for deployment 11 (Fig. 11a) show the typical three-layer structure for late fall conditions, when a layer of cold "winter water" was sandwiched between the warm surface layer and the warm layer below the halocline (*see* discussion of Fig. 2 above). Small-scale temperature anomalies are indicative for intrusions throughout the measurement range of the profiler, with particularly vigorous intrusions found in the first week of January in the depth range 80–120 m, which coincides with the core of the HTZ. Different from the cold intrusions found in most of the examples discussed above, the intrusions in deployment 11 show a positive temperature anomaly.

The rate at which waters with different temperatures are mixed by molecular heat conduction at the smallest (centimeter to decimeter) scales is usually (e.g., Thorpe 2005) quantified with the help of the temperature variance decay rate,

$$\chi = 6\kappa_\theta \left\langle \left(\frac{\partial \Theta \prime}{\partial z} \right)^2 \right\rangle, \tag{1}$$

where κ_θ is the molecular diffusivity of heat. Here, angular brackets denote the average over a small vertical depth interval (1.0 m in our case), and primes indicate deviations from this

average. Note that in Eq. 1, we assume isotropy at the smallest scales to express temperature gradients in all spatial directions in terms of the vertical gradient alone. If the conditions for small-scale isotropy are not satisfied (this is often the case, as shown below), expression 1 still provides a useful measure for the mixing of small-scale vertical temperature gradients by molecular diffusion. Figure 11b shows that high mixing rates are found particularly inside the thermocline region, and in the vicinity of warm intrusions. One could interpret the latter as an indication of enhanced turbulence in the vicinity of intrusions, in analogy to dense gravity currents entering the basin, where turbulence and mixing are strongly increased at the interface of the gravity current (Schmale et al. 2016); however, as shown in the following, this is generally not the case.

The standard approach (e.g., Thorpe 2005) to estimate turbulence parameters from temperature microstructure data relies on fitting observed temperature gradient spectra to a theoretical model spectrum (the Batchelor spectrum), using χ and the turbulence energy dissipation rate, ε, as fitting parameters. Once ε is known, the vertical turbulent diffusivity can be computed from $K_z = \gamma \varepsilon / N^2$ with $\gamma = 0.2$ (Osborn 1980). This approach is, however, only valid under at least two conditions: (1) turbulence is energetic enough to overcome the damping effect of stratification, and (2) observed and theoretical model spectra sufficiently agree, indicating isotropic small-scale turbulence and an active spectral cascade of scalar variance. Condition (1) is usually quantified with the help of the buoyancy Reynolds number, $Re_b = \varepsilon (\nu N^2)^{-1}$, where ν is the

molecular viscosity. If Re_b is smaller than a critical threshold of order 10, the turbulent vertical mass flux is known to collapse, and thus $K_z = 0$ for the vertical turbulent diffusivity. Following Ivey and Imberger (1991) and Bouffard and Boegman (2013), we use a threshold of $Re_b = 15$ for this transition. Deviations of the observed spectra from the theoretical universal spectrum were measured with the help of the maximum-likelihood approach developed by Ruddick et al. (2000). Spectra with too large deviations were discarded. Further details are described in Holtermann et al. (2017), who used an identical method to study mixing during an MBI.

The main result of our analysis is that in the depth range of the HTZ (80–120 m depth) and based on a total of 92 profiles, only 19 out of 3680 (corresponding to 0.9%) turbulence estimates passed the above quality checks and the threshold for energetic turbulence. Averaging these estimates results in a mean value of $\varepsilon = 2 \times 10^{-8}$ W kg^{-1}. However, as 99.1% of all estimates indicated extremely weak turbulence (with $K_z = 0$ according to the above criteria), also the average of K_z over the entire deployment was close to zero. Similarly, low values were found in the deeper layer below the HTZ. This suggests that even during the energetic winter period with strong atmospheric forcing, vertical mixing due to shear-instabilities (e.g., due to breaking internal waves) in the stratified interior region of the basin is negligible. Also intrusions, usually thought to be associated with enhanced vertical current shear, did not show indications for enhanced turbulence. These findings are in line with a recent study by Holtermann et al. (2017), who used the same profiling system to study mixing under the particularly energetic conditions of an MBI. Also in their study, no significantly enhanced turbulence activity could be detected.

As temperature anomalies due to intrusions do vanish eventually as a result of mixing, the question arises where and by which other processes this mixing occurs. Boundary mixing processes, not detectable from our turbulence measurements in the center of the basin, provide one possible explanation. If the oxygen imported by lateral intrusions is mainly absorbed by the sediment, as our analysis in the following section suggests, then these intrusions will be directly exposed to boundary mixing. Data from a tracer release experiment (Holtermann et al. 2012; Holtermann and Umlauf 2012) have clearly shown that in the deeper part of the basin, boundary mixing provides by far the largest contribution to overall vertical mixing. Similarly, turbulence microstructure observations in the neighboring Bornholm Basin provided direct evidence for the importance of boundary mixing (Lappe and Umlauf 2016). It is likely that similar boundary mixing processes are effective in the HTZ of the Gotland Basin.

Our measurements also revealed a few alternative mixing processes that are represented in the temperature microstructure profile shown in Fig. 12a, obtained during a period with particularly strong intrusions in January 2015 (*see* Fig. 11 above). The most common situation in our data set is exemplified in Fig. 12b, which shows temperature fluctuations with decimeter to meter vertical scales. For energetic reasons, these scales are by far too large to be associated with active turbulence (Re_b well below 15); yet they are reflected in enhanced molecular mixing rates as shown in Fig. 11b. It may be speculated that these small-scale temperature fluctuations are caused by the disintegration of larger-scale intrusions, but the detailed mechanisms involved in this cascade process are unclear at the moment.

Another mixing process, diffusive convection, is likely more effective in mixing water masses of different temperatures. Diffusive convection is driven by differences in the molecular diffusivities of temperature and salinity in situations in which a stable salinity gradient is partly compensated by a gravitationally unstable temperature gradients (Radko 2013). In high-resolution temperature profiles, diffusive convection is typically characterized by step-like structures, where thin (centimeter-scale) interfaces separate nearly perfectly mixed vertical layers. The conditions for double diffusive convection can be expressed by the density ratio R_ρ:

$$R_\rho = \frac{\beta \Delta S_A}{\alpha \Delta \Theta},$$ (2)

with ΔS_A, $\Delta \Theta$ denoting the differences of absolute salinity and conservative temperature across a depth interval, α the thermal expansion coefficient, and β the haline contraction coefficient. In the ocean, diffusive staircases are typically found for density ratios in the range $1 < R_\rho < 10$ (Kelley et al. 2003).

In our data set, diffusive step structures are often observed at the upper edge of warm intrusions, or, vice-versa, at the lower edge of cold intrusions, where conditions are favorable for diffusive convection. A typical example is shown in Fig. 12c, illustrating a series of double-diffusive steps in the temperature microstructure data. While the response time of the conductivity sensor is too slow to fully resolve the diffusive interfaces (blue line), it does resolve the well-mixed steps. This allowed us to obtain reliable estimates of both $\Delta \Theta$ and ΔS_A to compute R_ρ. We follow the methodology of Umlauf et al. (2018) to calculate R_ρ, and find $1.3 < R_\rho < 4.0$. These values are fully in the range for which diffusive staircases are expected (Kelley et al. 2003).

Discussion

We start our discussion with the construction of volume and oxygen budgets for the HTZ. To this end, the HTZ is thought to be bounded at the top by the isopycnal surface A_{top}, and at the bottom by either the isopycnal surface A_{bot} or the sediment surface A_{sed}. In areas where the water depth is larger than the depth of the top isopycnal surface, A_{top}, the HTZ is laterally bounded by the vertical surface A_{lat} with outward unit normal vector **n**. With these assumptions, the volume V of the HTZ is described by the following relation:
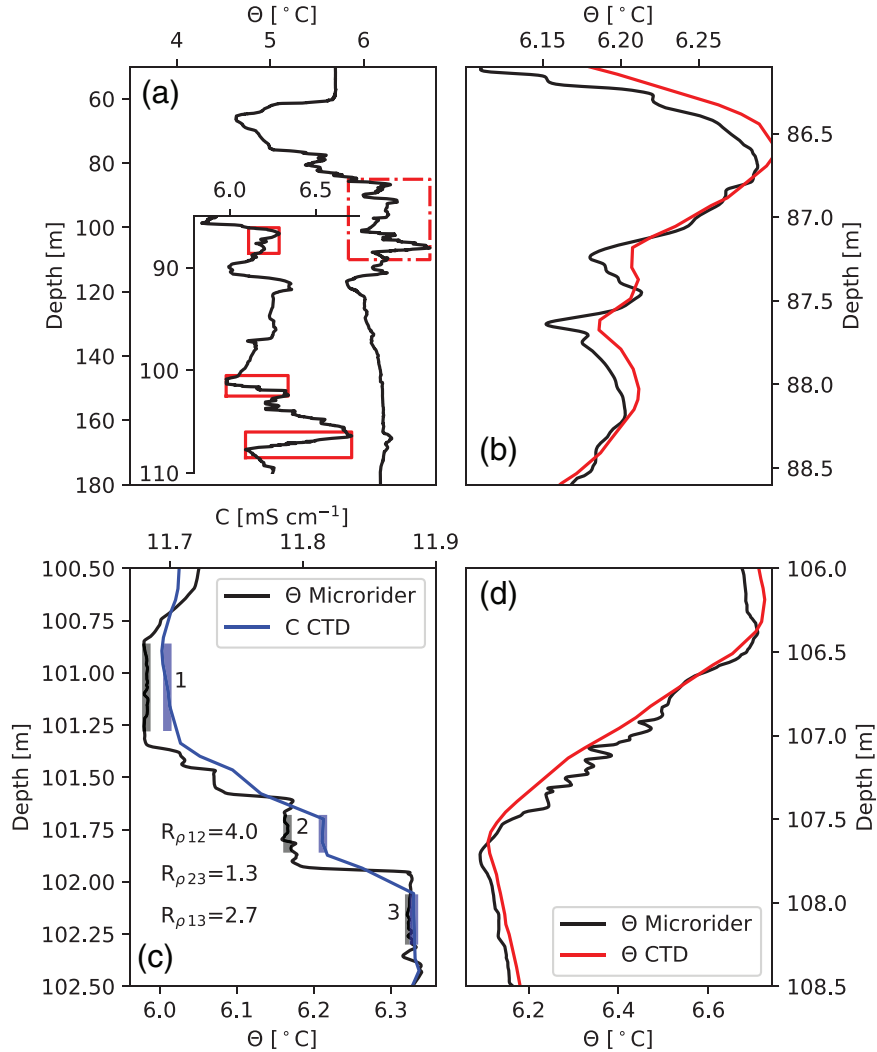
Fig. 12. Panel (**a**) shows the temperature profile marked in Fig. 11 (inset figure shows an enlarged version of the region inside the dash-dotted box). Panels (**b–d**) show vertical temperatures profiles from the standard CTD sensor (red) and fast thermistor (black), respectively, for the subregions marked by the red boxes in (**a**). Panel (**c**) includes conductivity data (blue) from the standard CTD sensor as a proxy for salinity. Lighter colored vertical lines in (**c**) mark the step regions used to estimate R_ρ. Each step is numbered, and the values of R_ρ for the corresponding interfaces between the steps are named accordingly, for example, $R_{\rho 23}$ is the density ratio of the interface between steps 2 and 3.

$$\frac{dV}{dt} = -\int_{A_{\mathrm{lat}}} \mathbf{u}\cdot\mathbf{n}\,dA + \int_{A_{\mathrm{top}}} w^*\,dA - \int_{A_{\mathrm{bot}}} w^*\,dA, \tag{3}$$

where $\mathbf{u}$ is the current velocity and $w^\star$ the vertical velocity of an isopycnal surface *relative* to the vertical current (we assume that isopycnals are approximately horizontal in this context). The first term on the right side denotes the advective transport of water across the lateral boundaries of the HTZ. The last two terms denote volume changes due to diabatic motions of the bounding isopycnal surfaces. If vertical mixing is negligible, isopycnal surfaces move exactly with the vertical current, and we thus have $w^\star = 0$. The last two terms in Eq. 3 vanish in this case.

Similarly, a budget for the oxygen content of the HTZ can be constructed:

$$\frac{d\langle C_{O_2}\rangle V}{dt} = -\int_{A_{\mathrm{lat}}} C_{O_2}\mathbf{u}\cdot\mathbf{n}\,dA + \int_{A_{\mathrm{top}}} \left(w^*C_{O_2} + K_z\frac{\partial C_{O_2}}{\partial z}\right)dA$$
$$- \int_{A_{\mathrm{bot}}} \left(w^*C_{O_2} + K_z\frac{\partial C_{O_2}}{\partial z}\right)dA - A_{\mathrm{sed}}d_{\mathrm{sed}} - VD, \tag{4}$$

where $\langle C_{O_2}\rangle$ is the volume-averaged oxygen concentration inside the HTZ. The first term on the right side describes the advective flux (e.g., due to intrusions) of oxygen across the lateral boundaries of the HTZ. Turbulent diffusion of oxygen through the upper and lower bounding isopycnal surfaces is parameterized by the turbulent eddy-diffusivity K_z. Finally, $d_{\mathrm{sed}} > 0$ denotes the sedimentary oxygen demand (averaged over A_{sed}), and $D > 0$ the volume-averaged oxygen consumption rate in the water column. In summary, Eq. 4 assumes that the change in total oxygen

content in the HTZ is balanced by: lateral exchange (intrusions); diapycnal turbulent diffusion through the top and bottom isopycnal surfaces (terms with K_z); vertical motion of the top and bottom bounding surfaces relative to the water (terms with $w*$); sedimentary oxygen demand; and oxygen consumption in the interior.

Estimating the oxygen consumption rate

We first consider the HTZ oxygen budget for the special situation encountered in spring/summer 2011, when oxygen concentrations decayed nearly linearly (Fig. 8b), and no indications for the lateral import of oxygen via intrusions were found (*see* Supplementary Material). This implies that the lateral transport term in Eq. 4 can be neglected. Based on the observed structure of the HTZ, analyzed in more detail in Appendix, we apply Eq. 4 to the core region of the HTZ, vertically delineated by two isopycnal surfaces with potential densities of 8.25 kg m^{-3} (A_top) and 8.90 kg m^{-3} (A_bot). The vertical positions of these isopycnal surfaces showed only little vertical variability in spring/summer 2011, suggesting that the volume V of the HTZ was approximately constant. Finally, we argue in Supplementary Material that stagnating temperatures and small vertical oxygen gradients inside the HTZ indicate that the mixing terms in Eq. 4 can be ignored.

With these assumptions, the oxygen budget in Eq. 4 reduces to an equation of the form

$$\frac{d\langle C_{O_2}\rangle}{dt} = -\frac{A_\text{sed}}{V}d_\text{sed} - D, \tag{5}$$

reflecting a simple balance between oxygen decay and consumption. For the 2011 spring/summer period, the magnitude of the rate term in Eq. 5 can be estimated from the observed oxygen decay in the HTZ. For Sta. TF271, located in the center of the basin, we showed in Section 3.4 that $dC_{O_2}/dt = 0.18\ \mu$mol L^{-1} d^{-1} (*see* Fig. 8b). To test the robustness and basin-scale relevance of this estimate, we also computed decay rates at the nearby Stas. TR263, TF260, TF272, TF270, and TF286 (from south to north, *see* Fig. 1). The results, compiled in Table 2, suggest that for all neighboring stations, except for the southernmost Sta. TF263, the observed decay rates vary by less than 10% around an average value of

0.165 μmol L^{-1} d^{-1}. At Sta. TF263, we found a substantially smaller decay rate (0.11 μmol L^{-1} d^{-1}), indicating that this remote station is not representative for the basin. For comparison, it should be noted that these values are less than half the typical deep-water oxygen decay rates in the Gotland Basin found by Holtermann et al. (2017) for the period after an MBI: 0.27 μmol L^{-1} d^{-1} at 215 m depth, and 0.81 μmol L^{-1} d^{-1} in 237 m depth (*see* their fig. 9a,b), which likely reflects the increasing ratio of sediment surface to water volume in the deepest part of the basin.

The geometric parameters required for the evaluation of Eq. 5 were determined as follows. First, as described in Supplementary Material, we computed the mean depths of the isopycnal surfaces bounding the core region of the HTZ at the top ($\approx$ 90 m depth) and bottom ($\approx$ 120 m). As the Gotland Basin is laterally not completely confined by topography at these depth levels, the assignment of horizontal boundaries for the HTZ volume is less straightforward. To investigate the sensitivity with respect to the assumed lateral extent of the HTZ, we tested two different configurations. In the first case, we assumed that the HTZ only extends over the "central" region of the Gotland Basin, as indicated in red in Fig. 1a. In the second case, we assumed an "extended" region, shown in brownish colors in Fig. 1b, in which the HTZ only has a single open boundary in the northern part of the area. The hypsographic parameters for both configurations are summarized in Table 3, showing that the hypsographic ratio $A_\text{sed}V^{-1}$ is slightly more than twice for the "extended" region, pointing at a relatively stronger impact of sedimentary oxygen demand.

If the basin-scale oxygen consumption is exclusively determined by the sedimentary oxygen demand (this assumption will be discussed below), the sedimentary uptake rate d_sed can be computed from Eq. 5, based on the observed oxygen decay rates and hypsographic parameters summarized in Tables 2 and 3, respectively. For the range of observed decay rates, and differences in the hypsographic parameter $A_\text{sed}V^{-1}$ for the "central" and "extended" HTZ areas, we find a range of sedimentary oxygen uptake rates of d_sed= 5.8–20 mmol m^{-2} d^{-1} (*see* Table 3). Our most realistic estimate of the uptake rate is d_sed^avg = 8.7 mmol m^{-2} d^{-1} (Table 3), using the average decay rate

Table 2. Oxygen concentrations and decay rates of several central Baltic Sea stations on the 8.5 kg m^{-3} isopycnal (center of the HTZ) for two different dates in spring/summer 2011.

Station	Date profile 1	Date profile 2	O$_2$ profile 1 (μmol L^{-1})	O$_2$ profile 2 (μmol L^{-1})	Oxygen decay rate (μmol L^{-1} d^{-1})
TF263	26 Mar 2011	07 Aug 2011	20.3	5.6	0.11
TF260	14 May 2011	08 Aug 2011	20.0	5.3	0.17
TF272	13 May 2011	27 Jul 2011	18.7	5.8	0.17
TF271	13 Mar 2011	23 Sep 2011	35.0	0.0	0.18
TF270	14 May 2011	10 Aug 2011	19.8	6.6	0.15
TF286	15 May 2011	28 Jul 2011	13.6	2.5	0.15

Table 3. Hypsographic parameter $A_{sed}V^{-1}$ and sedimentary oxygen demand d computed from the simplified HTZ oxygen budget in Eq. 5 for the depth range 90–120 m. Minimum and maximum values of d were computed based on the smallest and largest observed decay rates in Table 2, respectively. The average value of d is based on the average decay rate (0.165 μmol L^{-1} d^{-1}) of all stations, except Sta. TF263. The "central" and "extended" regions of the HTZ are indicated in red in Fig. 1a and in brown in Fig. 1b, respectively.

	Central	Extended
V (km^3)	363.8	566.9
A_{sed} (km^2)	3219	10,953
$A_{sed}V^{-1}$ (m^{-1})	0.009	0.019
d_{sed}^{min} (mmol m^{-2} d^{-1})	12.2	5.8
d_{sed}^{max} (mmol m^{-2} d^{-1})	20.0	9.5
d_{sed}^{avg} (mmol m^{-2} d^{-1})	18.3	8.7

of 0.165 μmol L^{-1} d^{-1} computed above, and assuming $A_{sed}V^{-1}$ for the "extended" area, which most realistically represents the relevant large-scale basin geometry.

It is instructive to compare the uptake rates in Table 3 to the experiments by Noffke et al. (2016), who estimated the sedimentary oxygen demand on the eastern slope of the Gotland Basin (positions shown in Fig. 1) with the help of in situ incubation experiments. Noffke et al. (2016) reported six incubations, conducted at 65–80 m depth, from which they found uptake rates between $d_{sed}=$ 5.8 mmol m^{-2} d^{-1} and $d_{sed}=$ 20.9 mmol m^{-2} d^{-1} with an average of 11.2 mmol m^{-2} d^{-1}. We thus note that the range of uptake rates found by Noffke et al. (2016) from in situ incubation experiments almost perfectly overlaps with the range of values ($d_{sed}=$ 5.8–20.0 mmol m^{-2} d^{-1}) identified from our budget approach. This range can be further constrained by only considering data from the deepest experiments ($\approx$ 80 m depth) investigated by Noffke et al. (2016), which are most representative for the conditions in the HTZ. Noffke et al. (2016) found $d_{sed}=$ 6–10 mmol m^{-2} d^{-1} at this depth level, which brackets our best estimate $d_{sed}^{avg} =$ 8.7 mmol m^{-2} d^{-1} for the uptake rate. This value is also not far from $d_{sed}=$ 7.8 mmol m^{-2} d^{-1}, found by Holtermann et al. (2017) from observed oxygen decay rates in the deepest layers of the Gotland Basin (below 140 m depth) after an MBI.

These results suggest that the sedimentary oxygen demand does not show a clear depth dependence, and is most likely the dominant term on the right side of Eq. 5. A more precise estimate of the relative importance of the interior oxygen consumption D and sedimentary uptake d_{sed} would require direct measurements of D, which are, however, not available at the moment.

Finally, it should be noted that the uptake rates computed above constitute lower bounds as they are based on the assumption that both intrusions and downward mixing of oxygen into the HTZ are insignificant during this period. The good agreement with the uptake rates measured by Noffke

et al. (2016) supports this assumption, however, with the following caveat. If the HTZ oxygen concentrations approach zero, the simplified budget in Eq. 5 breaks down. In this case, if the effect of intrusions remains negligible, the oxygen consumption is balanced by the downward mixing of oxygen into the HTZ. This type of balance is likely to hold in winter 2011/2012, when mixing was stronger compared to the summer period but oxygen concentrations stayed close to zero (Fig. 8b). In this situation, it is reasonable to expect an overall reduced HTZ oxygen turnover as the sedimentary oxygen uptake critically depends on concentration differences across the sediment–water interface. We conclude that even under conditions with maximum mixing and reduced uptake rates, the downward mixing of oxygen is not sufficient to maintain the HTZ. On the long-term average, the effect of mixing on the HTZ oxygen budget must therefore be significantly smaller than the effect of lateral intrusions, as discussed in more detail in the following.

The long-term impact of intrusions

We next use the budget expressions in Eqs. 3, 4 to estimate the amount of oxygen imported by intrusions on the long-term average. We start with the observation that on long (i.e., multi-annual) time scales, the density structure in the region below the halocline is approximately stationary. This implies that the gradual upwelling of isopycnals induced by intrusions into deeper layers (Stigebrandt 1987) is compensated by a downward mixing of lighter waters. We thus have $\bar{w} = -\bar{w}^*$, where here and in the following the overbar denotes a quantity that has been averaged over a long time scale and over an isopycnal surface (e.g., A_{top} and A_{bot}). Next, we note from Figs. 3 and 4 that, to first order and on multi-annual time scales, the volume, the oxygen content, and the location of the HTZ are approximately constant over time.

With these assumptions, the rate terms on left sides of Eqs. 3, 4 do not provide a significant contribution to the budgets, and can thus be neglected. If we further express the first integral on the right side of Eq. 3 as the difference between the volume flux Q^{in} entering the HTZ (via intrusions) and the volume flux Q^{out} leaving it at some other location, we can reexpress Eq. 3 as follows:

$$0 = Q^{in} - Q^{out} + \bar{w}_{top}^* A_{top} - \bar{w}_{bot}^* A_{bot}. \qquad (6)$$

The inflow by intrusions is thus balanced by lateral outflow at some other location, and by diapycnal mixing of fluid across the bounding isopycnal surfaces at the top and bottom of the HTZ. The diapycnal velocity $\bar{w}_{bot}^*$ is exclusively determined by the inflow Q_{deep}^{in} into the layers below the lower bounding isopycnal surface: $\bar{w}_{bot}^* = -Q_{deep}^{in}/A_{bot}$. Assuming a net import of waters due to the effect of intrusions ($Q_{deep}^{in} > 0$ and $Q^{in} + Q_{deep}^{in} > Q^{out}$), we have $\bar{w}_{top}^* < 0$ and $\bar{w}_{bot}^* < 0$.

Similarly, we formulate the long-term averaged version of the HTZ oxygen budget in Eq. 4 as follows:

$$0 = Q^{\text{in}}C_{\text{O}_2}^{\text{in}} - Q^{\text{out}}C_{\text{O}_2} + \bar{w}_{\text{top}}^{*}A_{\text{top}}C_{\text{O}_2} - \bar{w}_{\text{bot}}^{*}A_{\text{bot}}C_{\text{O}_2}^{\text{bot}} - \bar{F}_{\text{top}}A_{\text{top}} \\ + \bar{F}_{\text{bot}}A_{\text{bot}} - VD_{\text{net}}, \quad (7)$$

where $\bar{F}_{\text{top}}$ and $\bar{F}_{\text{bot}}$ denote the averaged diffusive oxygen fluxes at the top and bottom of the HTZ, and $VD_{\text{net}} = A_{\text{sed}}d_{\text{sed}} + VD$ the (constant) net consumption rate. In Eq. 7, we assumed that waters entering the HTZ via intrusions have the oxygen concentration $C_{\text{O}_2}^{\text{in}}$, while waters leaving the HTZ, laterally or vertically across the upper bounding isopycnal surface, are characterized by the average concentration, C_{O_2}, inside the HTZ. The concentration of waters entering the HTZ by mixing across the lower boundary are assumed to have the concentration $C_{\text{O}_2}^{\text{bot}}$. Using Eq. 6 and $\bar{w}_{\text{bot}}^{*}A_{\text{bot}} = -Q_{\text{deep}}^{\text{in}}$ derived above, Eq. 7 can be written as

$$0 = Q^{\text{in}}\left(C_{\text{O}_2}^{\text{in}} - C_{\text{O}_2}\right) + Q_{\text{deep}}^{\text{in}}\left(C_{\text{O}_2}^{\text{bot}} - C_{\text{O}_2}\right) - \bar{F}_{\text{top}}A_{\text{top}} + \bar{F}_{\text{bot}}A_{\text{bot}} - VD_{\text{net}}. \quad (8)$$

To estimate the relative importance of the first two terms on the right side, we first note that the concentration differences appearing in these terms are of the same order of magnitude. Stigebrandt (1987) showed that for periods without MBIs, intrusions rarely reach layers deeper than the lower edge of the HTZ (*see* their fig. 8), which implies $Q^{\text{in}} \gg Q_{\text{deep}}^{\text{in}}$. The second term on the right side of Eq. 8 is thus negligible. The vertical flux terms $\bar{F}_{\text{top}}$ and $\bar{F}_{\text{bot}}$ cannot be neglected in general. However, as discussed at the end of Section 4.1, oxygen concentrations close to zero in the winter period 2011/2012 (Fig. 8b), when wind-driven mixing reached its maximum, suggest that the effect of these terms is significantly smaller than the effect of intrusions.

To first order, the long-term averaged flux of oxygen into the HTZ can thus be written as

$$Q^{\text{in}}C_{\text{O}_2}^{\text{in}} = \frac{r}{r-1}VD_{\text{net}}, \quad (9)$$

where we have introduced the concentration ratio $r = C_{\text{O}_2}^{\text{in}}/C_{\text{O}_2}$. Expression (9) shows that the total oxygen flux into the HTZ can be estimated based on the oxygen consumption rates computed in Section 4.1 above, assuming that these rates remain stable over multi-annual time scales. This is likely a good approximation, as consumption rates computed for different years and locations, and using different methods, were shown to converge. A lower bound for the pre-factor $r/(r-1)$ in Eq. 9 is easily derived from the observation that oxygen concentrations of intrusions rarely exceed twice the ambient concentrations inside the HTZ (*see*, e.g., Fig. 6), suggesting that $r = 2$ is at the upper end of the plausible range of values.

The corresponding pre-factor $r/(r-1) = 2$ is thus a lower bound, resulting in a conservative estimate of the oxygen imported by intrusions. Analogously to Section 4.1, we assume that the HTZ is vertically bounded by isopycnal surfaces with potential densities of 8.25 and 8.90 kg m^{-3}, respectively. The corresponding average depths of these isopycnals were 94 and 122 m for the period from March 2008 until November 2014. The HTZ volumes between these two isopycnals were 498 km^3 for the "extended" area and 378 km^3 for the "central" area.

Assuming the lowest decay rate found in Table 2 (0.11 μmol L^{-1} d^{-1}) and the "central" volume, we find from Eq. 9 that even with this most conservative estimate approximately 30 Gmol of oxygen are imported per year into the HTZ. For the parameters that we consider as the most realistic (station-averaged decay rate of 0.165 μmol L^{-1} d^{-1} and "extended" HTZ volume), this amount increases to 60 Gmol per year. It is instructive to compare these numbers to the 21 Gmol imported by the MBI 2015 (Holtermann et al. 2017), which was considered to be one of the strongest events of this type since the beginning of the records. As MBIs occur on an approximately decadal time scale, we conclude that, on the long-term average, the amount of oxygen imported by intrusions is one order of magnitude larger than that imported by MBIs. While uncertainties in the oxygen uptake rates and the effects of mixing may have a significant effect on the HTZ oxygen budget (see above), they are unlikely to affect this order-or-magnitude estimate.

Conclusions

Figure 13 summarizes the main results of our study, suggesting that lateral intrusions rather than turbulent downward transport of oxygen are the dominant process maintaining the HTZ in the central Baltic Sea. Sedimentary oxygen demand was identified as the most important oxygen sink for the HTZ, with a small, but at the moment otherwise unconstrained, contribution from oxygen consumption in the water column. While small, the role of consumption within the water column is recently discussed as a factor for changing oxygen decay rates between different MBIs (Meier et al. 2018). This points to the need for experiments quantifying this part of the oxygen budget. Although the observed sedimentary oxygen rates of (Noffke et al. 2016) show an excellent agreement with the calculated rates of our budget, the overall amount of in-situ measurements is extremely limited at the moment.

A detailed analysis of decaying oxygen concentrations in the HTZ during an exceptional period with negligible intrusion activity in summer 2011 suggests an average oxygen decay rate of 0.165 μmol L^{-1} d^{-1} with an uncertainty, based on the comparison of different stations, of less than 10%. For typical oxygen concentrations of 20–30 μmol L^{-1}, this corresponds to a HTZ decay time scale of approximately half a year,
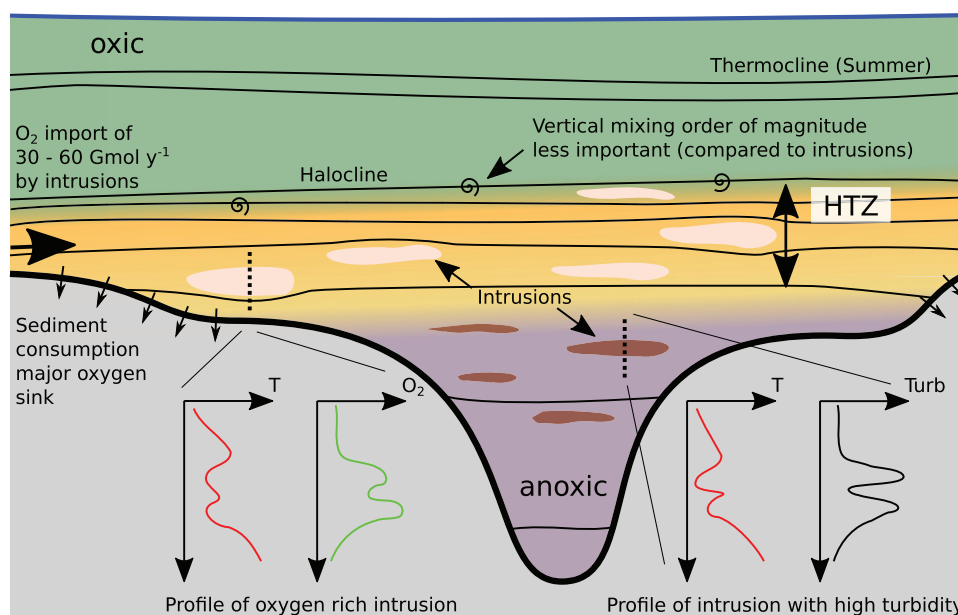
Fig. 13. Conceptual sketch of processes controlling the HTZ in the central Baltic Sea.

consistent with the time scale for the observed collapse of the HTZ in the years 2011/2012, when only weak intrusions were observed. A second major conclusion is that, irrespective of internal or boundary mixing processes and their seasonal variability, vertical downward mixing of oxygen is not sufficient to maintain the HTZ. This does not imply that the oxygen flux through the halocline is zero (in view of the strong oxygen gradients in the halocline this is not expected), but it does show that mixing merely provides a modification of the HTZ oxygen budget compared to the dominant sources and sinks. Without detailed investigations of boundary mixing processes, this contribution cannot be quantified at the moment.

Different from the current believe that the oxygen budget in the deep-water region below the halocline is largely controlled by the cumulative effect of MBIs, sporadically occurring on a decadal time scale, we found that the amount of oxygen imported by intrusions into the HTZ exceeds that imported by MBIs in the entire deep-water region of the Gotland Basin by approximately one order of magnitude. This highlights the HTZ as a hotspot for biogeochemical turnover, which is in line with some recent studies (Noffke et al. 2016; Sommer et al. 2017) focusing on the importance of the HTZ for basin-wide nutrient recycling. As shown in Section 3.4, intrusions also control the stability of the HTZ, with far-reaching consequences for the spatial distribution of anoxic areas. During periods with normal intrusion activity, the anoxic region below the HTZ typically does not reach depth levels higher than 130 m (Figs. 3c and 4c), which corresponds to an anoxic area of 11,000 km^2 inside the "extended" region shown in Fig. 1b. This anoxic area, sometimes referred to as the "death zone" of the Baltic Sea, expands more than double

to 28,900 km^2 if the HTZ collapses, and the anoxic region expands up to 80 m depth (*see* deployment 5 in Fig. 3c). While the expansion of the Baltic Sea's anoxic areas in the past century has been mainly attributed to eutrophication (e.g., Carstensen et al. 2014), this suggests that physical factors also provide an important control on the extent of hypoxic areas.

Our long-term observations have shown that intrusions entering the Gotland Basin are not confined to the depth levels of the HTZ but could also frequently be observed in the deeper anoxic/sulfidic layers. Such intrusions did occasionally contain small amounts of oxygen but were more typically characterized by enhanced turbidity (*see* Fig. 13). As discussed above, we believe that these intrusions reflect the final stage of formerly oxic waters that have lost their oxygen along their path into the deep layers of the Gotland Basin. In this view, the enhanced turbidities are interpreted as the optical signature of colloidal sulfur particles generated during the mixing of oxic and sulfidic waters (Schmale et al. 2016; Holtermann et al. 2017), similar to the classical redoxcline turbidity peak found in the Baltic Sea and other euxinic systems (Blumenberg et al. 2007; Wakeham et al. 2012; Jakobs et al. 2014). This is consistent with a recent study of Beier et al. (2019), who investigated the microbiological consequences of permanent small-scale intrusions into the anoxic deep layers of the Gotland Basin. These authors describe an unexpected upregulation of oxygen-dependent genes in regions where neither oxygen nor oxygenated compounds such as nitrate and nitrite could be detected. Beier et al. (2019) argue that the most likely explanation for the puzzling transcription of denitrifying and sulfur oxidizing genes in the anoxic/sulfidic

region below the HTZ is a permanent stimulation by intrusions.

While we focused mainly on the role of intrusions for the HTZ oxygen budget, these studies suggest that the permanent disturbance of the water column by lateral intrusions might have a broader and more profound impact on the biogeochmistry of the redox transition zone that has not received sufficient attention in the past.

References

Astor, Y., F. Muller-Karger, and M. I. Scranton. 2003. Seasonal and interannual variation in the hydrography of the Cariaco Basin: Implications for basin ventilation. Cont. Shelf Res. **23**: 125–144. doi:10.1016/S0278-4343(02)00130-9

Axell, L. B. 1998. On the variability of Baltic Sea deepwater mixing. J. Geophys. Res. **103**: 21667–21682. doi:10.1029/98JC01714

Beier, S., P. L. Holtermann, D. Numberger, T. Schott, L. Umlauf, and K. Jürgens. 2019. A metatranscriptomics-based assessment of small-scale mixing of sulfidic and oxic waters on redoxcline prokaryotic communities. Environ. Microbiol. **21**: 584–602. doi:10.1111/1462-2920.14499

Blumenberg, M., R. Seifert, and W. Michaelis. 2007. Aerobic methanotrophy in the oxic–anoxic transition zone of the Black Sea water column. Org. Geochem. **38**: 84–91. doi:10.1016/j.orggeochem.2006.08.011

Bouffard, D., and L. Boegman. 2013. A diapycnal diffusivity model for stratified environmental flows. Dynam. Atmos. Oceans **61–62**: 14–34. doi:10.1016/j.dynatmoce.2013.02.002

Breitburg, D., and others. 2018. Declining oxygen in the global ocean and coastal waters. Science **359**: eaam7240. doi:10.1126/science.aam7240

Carstensen, J., J. H. Andersen, B. G. Gustafsson, and D. J. Conley. 2014. Deoxygenation of the Baltic Sea during the last century. PNAS **111**: 5628–5633. doi:10.1073/pnas.1323156111

Conley, D. J., and others. 2009*a*. Hypoxia-related processes in the Baltic Sea. Environ. Sci. Technol. **43**: 3412–3420. doi:10.1021/es802762a

Conley, D. J., J. Carstensen, R. Vaquer-Sunyer, and C. M. Duarte. 2009*b*. Ecosystem thresholds with hypoxia, p. 21–29. *In* Eutrophication in coastal ecosystems. Springer. doi:10.1007/978-90-481-3385-7_3

Dellwig, O., and others. 2010. A new particulate Mn–Fe–P-shuttle at the redoxcline of anoxic basins. Geochim. Cosmochim. Acta **74**: 7100–7115. doi:10.1016/j.gca.2010.09.017

Diaz, R. J., and R. Rosenberg. 2008. Spreading dead zones and consequences for marine ecosystems. Science **321**: 926–929. doi:10.1126/science.1156401

Feistel, R., G. Nausch, and N. Wasmund [eds.]. 2008. State and evolution of the Baltic Sea, 1952-2005. A detailed 50-year survey of meteorology and climate, physics, chemistry, biology, and marine environment. Hoboken, NJ: Wiley-Interscience.

Feistel, R., and others. 2010. Density and absolute salinity of the Baltic Sea 2006–2009. Ocean Sci. **6**: 3–24. doi:10.5194/os-6-3-2010

Fuchsman, C. A., J. W. Murray, and J. T. Staley. 2012. Stimulation of autotrophic denitrification by intrusions of the bosporus plume into the anoxic Black Sea. Front. Microbiol. **3**: 14. doi:10.3389/fmicb.2012.00257

Gargett, A. E. 1984. Vertical Eddy diffusivity in the ocean interior. J. Mar. Res. **42**: 359–393. doi:10.1357/002224084788502756

Gustafsson, B. G., and A. Stigebrandt. 2007. Dynamics of nutrients and oxygen/hydrogen sulfide in the Baltic Sea deep water. J. Geophys. Res. **112**: G02023. doi:10.1029/2006JG000304

Gustafsson, B. G., and others. 2012. Reconstructing the development of Baltic Sea eutrophication 1850–2006. Ambio **41**: 534–548. doi:10.1007/s13280-012-0318-x

Ho, T.-Y., G. T. Taylor, Y. Astor, R. Varela, F. Müller-Karger, and M. I. Scranton. 2004. Vertical and temporal variability of redox zonation in the water column of the Cariaco Basin: Implications for organic carbon oxidation pathways. Mar. Chem. **86**: 89–104. doi:10.1016/j.marchem.2003.11.002

Holtermann, P., and L. Umlauf. 2012. The Baltic Sea tracer release experiment. 2 Mixing processes. J. Geophys. Res. Oceans **117**: C01 022. doi:10.1029/2011JC007445

Holtermann, P., H. Burchard, U. Gräwe, K. Klingbeil, and L. Umlauf. 2014. Deep-water dynamics and boundary mixing in a non-tidal stratified basin. A modeling study of Baltic Sea. J. Geophys. Res. **119**: 1465–1487. doi:10.1002/2013JC009483

Holtermann, P. L., L. Umlauf, T. Tanhua, O. Schmale, G. Rehder, and J. J. Waniek. 2012. The Baltic Sea tracer release experiment: 1 Mixing rates. J. Geophys. Res. **117**: C01 021. doi:10.1029/2011JC007439

Holtermann, P. L., R. Prien, M. Naumann, V. Mohrholz, and L. Umlauf. 2017. Deep-water dynamics and mixing processes during a major inflow event in the bentral Baltic Sea. J. Geophys. Res. Oceans **122**: 6648–6667. doi:10.1002/2017JC013050

Ivey, G. N., and J. Imberger. 1991. On the nature of turbulence in a stratified fluid. Part I: The energetics of mixing. J. Phys. Oceanogr. **21**: 650–658. doi:10.1175/1520-0485(1991)021<0650:OTNOTI>2.0.CO;2

Jakobs, G., P. Holtermann, C. Berndmeyer, G. Rehder, M. Blumenberg, G. Jost, G. Nausch, and O. Schmale. 2014. Seasonal and spatial methane dynamics in the water column of the central Baltic Sea (Gotland Sea). Cont. Shelf Res. **91**: 12–25. doi:10.1016/j.csr.2014.07.005

Kamyshny, A., Jr., A. L. Zerkle, Z. F. Mansaray, I. Ciglenečki, E. Bura-Nakić, J. Farquhar, and T. G. Ferdelman. 2011. Biogeochemical sulfur cycling in the water column of a shallow stratified sea-water lake: Speciation and quadruple sulfur isotope composition. Mar. Chem. **127**: 144–154. doi:10.1016/j.marchem.2011.09.001

Keeling, R. F., A. Körtzinger, and N. Gruber. 2010. Ocean deoxygenation in a warming world. Ann. Rev. Mar. Sci. **2**: 199–229. doi:10.1146/annurev.marine.010908.163855

Kelley, D. E., H. J. S. Fernando, A. E. Gargett, J. Tanny, and E. Özsoy. 2003. The diffusive regime of double-diffusive convection. Prog. Oceanogr. **56**: 461–481. doi:10.1016/S0079-6611(03)00026-0

Konovalov, S. K., and others. 2003. Lateral injection of oxygen with the Bosporus plume—Fingers of oxidizing potential in the Black Sea. Limnol. Oceanogr. **48**: 2369–2376. doi:10.4319/lo.2003.48.6.2369

Konovalov, S. K., J. W. Murray, and G. I. W. Luther. 2005. Black Sea biogeochemistry. Oceanography **18**: 24–35. doi:10.5670/oceanog.2005.39

Lappe, C., and L. Umlauf. 2016. Efficient boundary mixing due to near-inertial waves in a Nontidal Basin: Observations from the Baltic Sea. J. Geophys. Res. Oceans **121**: 8287–8304. doi:10.1002/2016JC011985

Meier, H. E. M., and F. Kauker. 2003. Modeling decadal variability of the Baltic Sea: 2. Role of freshwater inflow and large-scale atmospheric circulation for salinity. J. Geophys. Res. **108**: 3368. doi:10.1029/2003JC001799

Meier, H. E. M., and others. 2006. Ventilation of the Baltic Sea deep water: A brief review of present knowledge from observations and models. Oceanologia **48**: 133–164.

Meier, H. E. M., G. Väli, M. Naumann, K. Eilola, and C. Frauen. 2018. Recently accelerated oxygen consumption rates amplify deoxygenation in the Baltic Sea. J. Geophys. Res. Oceans **123**: 3227–3240. doi:10.1029/2017JC013686

Meyer, D., U. Lips, R. D. Prien, M. Naumann, T. Liblik, I. Schuffenhauer, and D. E. Schulz–Bull. 2018. Quantification of dissolved oxygen dynamics in a semi-enclosed sea – A comparison of observational platforms. Cont. Shelf Res. **169**: 34–45. doi:10.1016/j.csr.2018.09.011

Millero, F. J., R. Feistel, D. G. Wright, and T. J. McDougall. 2008. The composition of standard seawater and the definition of the reference-composition salinity scale. Deep-Sea Res. I Oceanogr. Res. Pap. **55**: 50–72. doi:10.1016/j.dsr.2007.10.001

Naumann, M., V. Mohrholz, and J. J. Waniek. 2017. Water exchange between the Baltic Sea and the North Sea, and conditions in the Deep Basins. HELCOM Baltic Sea Environmental Fact Sheet Online, Tech. Report.

Noffke, A., S. Sommer, A. W. Dale, P. O. J. Hall, and O. Pfannkuche. 2016. Benthic nutrient fluxes in the eastern Gotland Basin (Baltic Sea) with particular focus on microbial mat ecosystems. J. Mar. Syst. **158**: 1–12. doi:10.1016/j.jmarsys.2016.01.007

Osborn, T. R. 1980. Estimates of the local rate of vertical diffusion from dissipation measurements. J. Phys. Oceanogr. **10**: 83–89. doi:10.1175/1520-0485(1980)010<0083:EOTLRO>2.0.CO;2

Prien, R. D., and D. E. Schulz-Bull. 2016. Technical note: GODESS – A profiling mooring in the Gotland Basin. Ocean Sci. **12**: 899–907. doi:10.5194/os-12-899-2016

Radko, T. 2013. Double-diffusive convection. Cambridge Univ. Press.

Reissmann, J., H. Burchard, R. Feistel, E. Hagen, H.-U. Lass, V. Mohrholz, G. Nausch, L. Umlauf, and G. Wieczorek. 2009. Vertical mixing in the Baltic Sea and consequences for eutrophication – A review. Progr. Oceanogr. **82**: 47–80. doi:10.1016/j.pocean.2007.10.004

Ruddick, B., A. Anis, and K. Thompson. 2000. Maximum likelihood spectral fitting: The Batchelor Spectrum. J. Atmos. Oceanic Tech. **17**: 1541–1555. doi:10.1175/1520-0426(2000)017<1541:MLSFTB>2.0.CO;2

Schmale, O., S. Krause, P. Holtermann, N. C. Power Guerra, and L. Umlauf. 2016. Dense bottom gravity currents and their impact on pelagic methanotrophy at oxic/anoxic transition zones. Geophys. Res. Lett. **43**: 5225–5232. doi:10.1002/2016GL069032

Schneider, B., G. Nausch, and C. Pohl. 2010. Mineralization of organic matter and nitrogen transformations in the Gotland Sea deep water. Mar. Chem. **119**: 153–161. doi:10.1016/j.marchem.2010.02.004

Sommer, S., D. Clemens, M. Yücel, O. Pfannkuche, P. O. J. Hall, E. Almroth-Rosell, H. N. Schulz-Vogt, and A. W. Dale. 2017. Major bottom water ventilation events do not significantly reduce basin-wide benthic N and P release in the eastern Gotland Basin (Baltic Sea). Front. Mar. Sci. **4**: 17. doi:10.3389/fmars.2017.00018

Stigebrandt, A. 1987. A model for the vertial circulation of the Baltic deep water. J. Phys. Oceanogr. **17**: 1772–1785. doi:10.1175/1520-0485(1987)017<1772:AMFTVC>2.0.CO;2

Stramma, L., G. C. Johnson, J. Sprintall, and V. Mohrholz. 2008. Expanding oxygen-minimum zones in the tropical oceans. Science **320**: 655–658. doi:10.1126/science.1153847

Thorpe, S. A. 2005. The Turbulent Ocean. Cambridge Univ. Press.

Umlauf, L., P. L. Holtermann, C. A. Gillner, R. D. Prien, L. Merckelbach, and J. R. Carpenter. 2018. Diffusive convection under rapidly varying conditions. J. Phys. Oceanogr. **48**: 1731–1747. doi:10.1175/JPO-D-18-0018.1

Wakeham, S. G., and others. 2012. Biomarkers, chemistry and microbiology show chemoautotrophy in a multilayer chemocline in the Cariaco Basin. Deep-Sea Res. I Oceanogr. Res. Pap. **63**: 133–156. doi:10.1016/j.dsr.2012.01.005

Wieczorek, G., E. Hagen, and L. Umlauf. 2008. Eastern Gotland Basin case study of thermal variability in the wake of deep water intrusions. J. Mar. Syst. **74**: S65–S79. doi:10.1016/j.jmarsys.2008.07.008

Zhurbas, V. M., and V. T. Paka. 1997. Mesoscale thermohaline variability in the eastern Gotland Basin following the 1993 Major Baltic inflow. J. Geophys. Res. Oceans **102**: 20917–20926. doi:10.1029/97JC00443

Zhurbas, V. M., and V. T. Paka. 1999. What drives thermohaline intrusions in the Baltic Sea? J. Mar. Syst. **21**: 229–241. doi:10.1016/S0924-7963(99)00016-0

Conflict of Interest

None declared.